MRI-based Methods for Quantification of Fat and Fatty Acid Composition. Validation and Applications.

Trinh, Lena

2020

Document Version:
Publisher's PDF, also known as Version of record

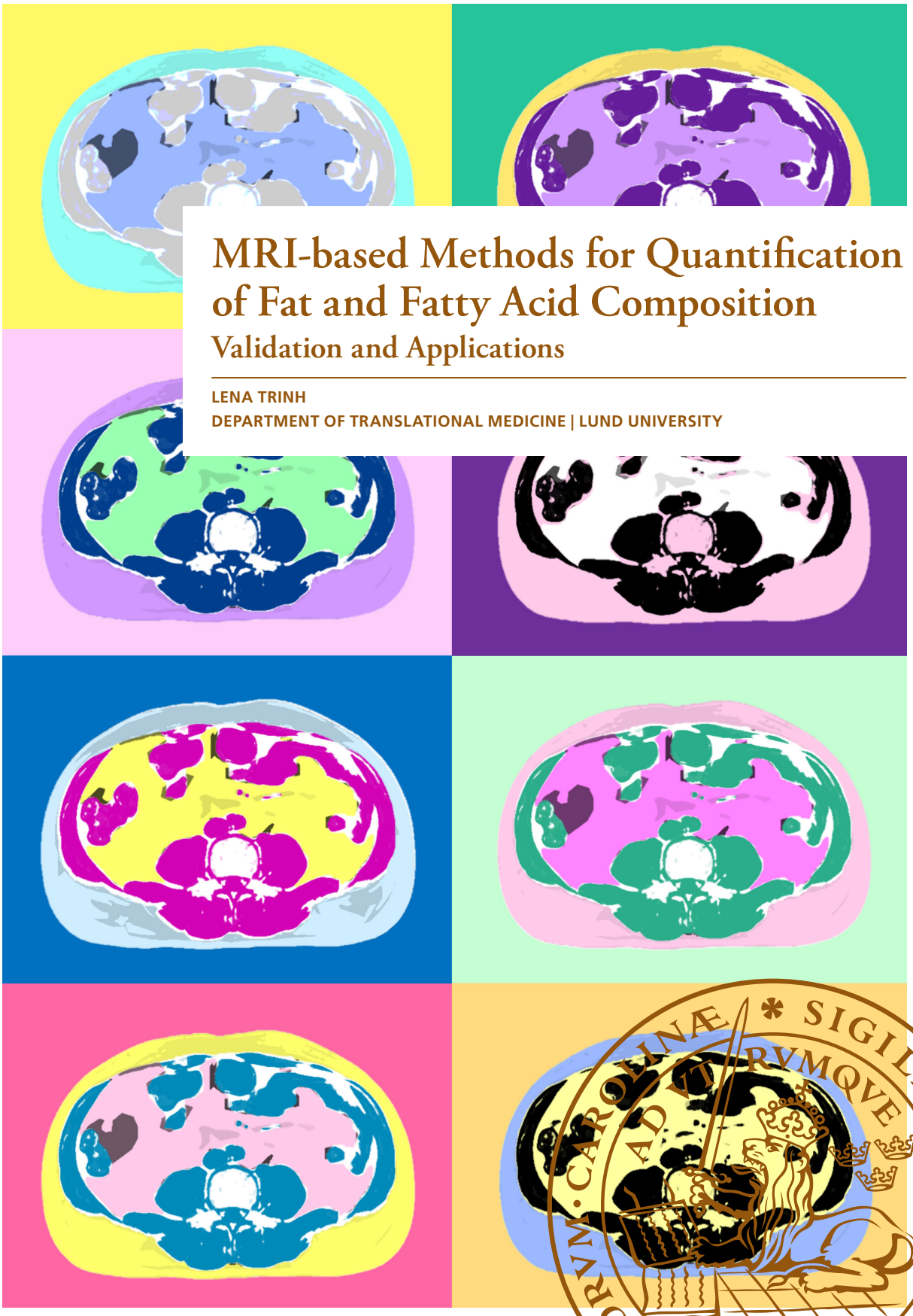

MRI-based Methods for Quantification of Fat and Fatty Acid Composition

Validation and Applications

LENA TRINH
DEPARTMENT OF TRANSLATIONAL MEDICINE | LUND UNIVERSITY

MRI-based Methods for Quantification of Fat and Fatty Acid Composition

MRI-based Methods for Quantification of Fat and Fatty Acid Composition

Validation and Applications

Lena Trinh

LUND
UNIVERSITY

DOCTORAL DISSERTATION

by due permission of the Faculty of Medicine, Lund University, Sweden.
To be defended at Agardhsalen, CRC, Friday June 5, 2020, at 9:15 am.

Faculty opponent
Professor Peter Lundberg, Linköping University

Organization LUND UNIVERSITY	**Document name** DOCTORAL THESIS
	Date of issue: 2020-06-05
Author: Lena Trinh	Sponsoring organization

MRI-based Methods for Quantification of Fat and Fatty Acid Composition – Validation and Applications

The interest of *in vivo* measurements of fat has increased over the years due to the increasing prevalence of obesity and obesity-related conditions such as diabetes, cardiovascular disease, and fatty liver. The relationship between the accumulation of adipose tissue within the different depots and organs of the body, and the risk of developing numerous diseases, has been investigated and established. However, the role of the fatty acid composition (FAC) of the adipose tissue in various diseases is yet to be settled and understood. In this thesis, MR-based methods for *in vivo* quantification of fat content and fatty acid composition have been investigated. Possible applications have been explored as well.

Today, the most widely used methods for assessing fat are based on magnetic resonance imaging (MRI). In some cases, MRI is even considered gold standard and one of the most common MRI-methods is water/fat imaging. Water/fat imaging has the possibility of measuring both the adipose tissue volume in depots designated for fat storage and the fat and adipose tissue within organs or body parts such as the liver or skeletal muscle. For example, the fat accumulation in skeletal muscle of patients with lymphedema was estimated using water/fat imaging in Paper II. Excess fat was found in both the intermuscular and intramuscular compartments of the edematous limbs. The excess accumulation of fat within the intermuscular and intramuscular compartments has not been demonstrated in any previous study of lymphedema.

Although widely used, water/fat imaging may be limited in some applications if a very high spatial resolution is desirable. In Paper I, an alternative T_2-based MRI method for estimating fat content using high spatial resolution MR images of the calf was explored. Different fitting algorithms were investigated and compared to low resolution water/fat imaging (reference method). While all approaches resulted in qualitatively adequate fat fraction images, only a non-linear least squares based fitting approach showed good agreement and correlation to the reference method.

Recently, MR-based methods for estimating the chemical composition of fat, i.e. the FAC, have been introduced. In contrast to the gold standard technique for measuring FAC (gas chromatography), MR-based approaches are non-invasive and offer spatial information without the need for multiple measurements. In this thesis, MR-based methods for *in vivo* FAC measurements were compared and validated against FAC quantification gas chromatography analysis of subcutaneous adipose tissue (Paper III). Especially the MRI-based approach resulted in promising results as high correlations to gas chromatography were found.

Several studies have suggested an association between FAC and the development of e.g. cardiovascular disease. In a previous study, a higher prevalence of hypertension (one of the strongest risk factors for cardiovascular disease) was found among Iraqi-born men resident in Sweden compared to Swedish-born men. In this thesis, the FAC of the subcutaneous and visceral adipose tissue of Iraqi- and Swedish-born men was measured and compared using the MRI-based method (Paper IV). Significantly different FAC was found between the studied groups. In general, higher proportions of polyunsaturated fat and lower proportions of saturated and monounsaturated fat were found among the Iraqi-born men.

Key words: MRI, MRS, fatty acid, fat quantification, adipose tissue, subcutaneous, visceral, water/fat imaging, chemical shift, T_2-relaxation, lymphedema, hypertension

Classification system and/or index terms (if any)

Supplementary bibliographical information		**Language** English
ISSN and key title: 1652-8220		**ISBN:** 978-91-7619-929-9
Recipient's notes	**Number of pages** 66	Price
	Security classification	

Signature  Date 2020-04-29

MRI-based Methods for Quantification of Fat and Fatty Acid Composition

Validation and Applications

Lena Trinh

LUND
UNIVERSITY

Cover image by Lena Trinh

Faculty of Medicine
Department of Translational Medicine

ISBN 978-91-7619-929-9
ISSN 1652-8220

Printed in Sweden by Media-Tryck, Lund University
Lund 2020

To the young Kevin Bacon

Table of Contents

Abstract

The interest of *in vivo* measurements of fat has increased over the years due to the increasing prevalence of obesity and obesity-related conditions such as diabetes, cardiovascular disease, and fatty liver. The relationship between the accumulation of adipose tissue within the different depots and organs of the body, and the risk of developing numerous diseases, has been investigated and established. However, the role of the fatty acid composition (FAC) of the adipose tissue in various diseases is yet to be settled and understood. In this thesis, MR-based methods for *in vivo* quantification of fat content and fatty acid composition have been investigated. Possible applications have been explored as well.

Today, the most widely used methods for assessing fat are based on magnetic resonance imaging (MRI). In some cases, MRI is even considered gold standard and one of the most common MRI-methods is water/fat imaging. Water/fat imaging has the possibility of measuring both the adipose tissue volume in depots designated for fat storage and the fat and adipose tissue within organs or body parts such as the liver or skeletal muscle. For example, the fat accumulation in skeletal muscle of patients with lymphedema was estimated using water/fat imaging in **Paper II**. Excess fat was found in both the intermuscular and intramuscular compartments of the edematous limbs. The excess accumulation of fat within the intermuscular and intramuscular compartments has not been demonstrated in any previous study of lymphedema.

Although widely used, water/fat imaging may be limited in some applications if a very high spatial resolution is desirable. In **Paper I**, an alternative T_2-based MRI method for estimating fat content using high spatial resolution MR images of the calf was explored. Different fitting algorithms were investigated and compared to low resolution water/fat imaging (reference method). While all approaches resulted in qualitatively adequate fat fraction images, only a non-linear least squares based fitting approach showed good agreement and correlation to the reference method.

Recently, MR-based methods for estimating the chemical composition of fat, i.e. the FAC, have been introduced. In contrast to the gold standard technique for measuring FAC (gas chromatography), MR-based approaches are non-invasive and offer spatial information without the need for multiple measurements. In this thesis, MR-based methods for *in vivo* FAC measurements were compared and validated against FAC quantification gas chromatography analysis of subcutaneous adipose tissue (**Paper III**). Especially the MRI-based approach resulted in promising results as high correlations to gas chromatography were found.

Several studies have suggested an association between FAC and the development of e.g. cardiovascular disease. In a previous study, a higher prevalence of hypertension (one of the strongest risk factors for cardiovascular disease) was found among Iraqi-born men resident in Sweden compared to Swedish-born men. In this

thesis, the FAC of the subcutaneous and visceral adipose tissue of Iraqi- and Swedish-born men was measured and compared using the MRI-based method (**Paper IV**). Significantly different FAC was found between the studied groups. In general, higher proportions of polyunsaturated fat and lower proportions of saturated and monounsaturated fat were found among the Iraqi-born men.

Populärvetenskaplig sammanfattning

Enligt Världshälsoorganisationen (WHO) är det idag fler i världen som dör på grund av fetma och fetmarelaterade sjukdomar än som dör på grund av undernäring. På 40 år har antalet människor med fetma ökat trefaldigt och det uppskattas att 39% av världens vuxna är överviktiga (BMI $\geq$ 25 kg/m^2), varav 13% är feta (BMI $\geq$ 30 kg/m^2). Fetma är associerad med ökad risk för att utveckla flertalet sjukdomar, exempelvis diabetes typ 2, hjärt- och kärlsjukdomar, fettlever och cancer. Med den ökande frekvensen av fetma och fetmarelaterade sjukdomar har även intresset för att mäta och studera kroppsfett ökat. Detta eftersom de exakta sambanden mellan kroppsfett och utvecklingen av dessa sjukdomar inte är fullt förstådda.

Det finns flera metoder för att lokalisera och mäta mängden kroppsfett. Den vanligaste metoden, som också anses vara ”gold standard” (d.v.s. den metod som är närmast sanningen), är mätningar med magnetresonanstomografi (MR). Med hjälp av MR-kameror kan man alltså avbilda och mäta kroppsfett utan invasiva ingrepp eller joniserande strålning. En av de vanligaste MR-metoderna för att mäta fett är ”water/fat imaging”, som är en kvantitativ metod. I den här avhandligen har metoder för att mäta fett med hjälp av magnetresonanstomografi (MR) undersökts och använts för att studera kroppens fett.

När det kommer till mycket högupplösta, kvantitativa fettbilder kan water/fat imaging vara begränsad. Högupplösta bilder kan vara av intresse vid studier av fettinlagrig i muskler om man t. ex. vill kunna skilja på de olika muskelgrupperna. En alternativ MR-metod för att få högupplösta fetthaltsbilder utreddes därför i delarbete 1. Generellt sett fanns det god överrensstämmelse mellan de högupplösta fettkvantifikationsbilderna och referensmetoden (lågupplöst water/fat imaging).

Lymfödem är en sjukdom som kännetecknas av ett defekt lymfsysten som resulterar i otillräcklig bortförsel av lymfvätska från det drabbade området (ofta ett ben eller en arm). Detta leder till en ansamling av lymfvätska och underhudsfett. Nyligen visade en studie att det även ansamlas fett i musklerna och inte bara under huden hos det sjuka benet eller armen. I delarbete 2 har water/fat imaging använts för att mäta det intramuskulära fettet (fettet inuti musklerna) och det intermuskulära fettet (fettet mellan musklerna) hos lymfödempatienter för att studera exakt var fettet ansamlas. Studien visade att ett överskott av fett ansamlas i både det intramuskulära och det intermuskulära området i det sjuka benet. Dessutom hittades inga samband mellan andra mått, t. e.x. mängd underhudsfett, och mängden fett i det intermuskulära och intramuskulära området. Detta tyder på att undersökningar med water/fat imaging kan vara nödvändiga för att kunna uppskatta mängden intermuskulärt och intramuskulärt fett.

Utöver mängd och var på kroppen som fettet ansamlas kan även fettets kemiska sammansättning, d.v.s. hur mättat, enkelomättat eller fleromättat fettet är, påverka för sjukdomsrisken. Gold standard för att mäta fettsammansättning är med hjälp av

gaskromatografi. Dock så kräver gaskromatografi minst ett vävnadsprov, d.v.s. gaskromatografi är en invasiv metod.

Som ett alternativ har en MR-baserad metod för att mäta fettets kemiska sammansättning utvecklats. Metoden, som är baserad på water/fat imaging-tekniken, är relativt ny och för att säkert veta att metoden fungerar måste den först testas mot en oberoende och etablerad metod (gaskromatografi). Detta har tidigare huvudsakligen gjorts med hjälp av vegetabiliska oljor. I delarbete 3 jämfördes därför den MR-baserade metoden med vävnadsprover av underhudsfett som analyserats med gaskromatografi (gold standard för att mäta fettsammansättning). Studien visade på starka korrelationer mellan metoderna vilket indikerar att den MR-baserade metoden kan mäta kroppfettets sammansättning korrekt.

Den MR-baserade metoden för att mäta fettsammansättning användes sedan i delarbete 4 för att mäta och jämföra den kemiska sammansättningen i underhuds- och bukfett hos irakiskfödda och svenskfödda män bosatta i Sverige. Detta då tidigare studier har visat att irakiskfödda bosatta i Sverige har en lägre frekvens av högt blodtryck trots att de har en högre risk för diabetes typ 2 jämfört av gruppen med svenskfödda män. Då högt blodtryck annars är associerat med diabetes typ 2 är det av intresse att utreda andra eventuella skillnader som kan förklara den lägre frekvensen av högt blodtryck hos de irakiskfödda männen, såsom den kemiska sammansättningen av fett. En signifikant högre andel fleromättat fett och signifikant lägre andelar mättat och enkelomättat fett uppmättes hos de irakiskfödda jämfört med de svenskfödda. Detta skulle kunna bero på skillnader i kost eller fettmetabolism, men då studiegrupperna var små så är det svårt att dra några generella och definitiva slutsatser i nuläget.

Sammanfattningsvis så visar det här arbetet att water/fat imaging kan vara ett bra verktyg för att studera fettansamlingen i muskler hos lymfödempatienter och att den MR-baserade metoden för att mäta fettets kemiska sammansättning kan fungera som en alternativ metod till gaskromatografi.

Acknowledgements

First, I would like to thank my supervisor Sven Månsson for giving me this opportunity and for always taking the time to answer all my questions, even the stupid ones and those I mumble while thinking out loudly. Thank you for letting me try out my own ideas but also for stopping me before I get stuck in endless optimization spirals.

Next, I would like to say thank you to my co-supervisors Pernilla Peterson, Håkan Brorson, Lars E Olsson, and Jonas Svensson, for supporting me with your expertise, enthusiasm, and videos of surgical treatments of lymphedema before modern liposuction. Extra thanks to Pernilla for being an excellent simultaneous supervisor and office mate, and fellow Singapore airport tourist.

Thanks to all my co-writers Emelie Lind, Peter Leander, Louise Bennet, and Karin Stenkula, for your invaluable feedback and knowledge which you have so generously shared with me.

Also, thanks to all my colleagues at Medical Radiation Physics for keeping me company, and well-fed with cakes and chili, during my years as a PhD student. Thanks to Viveca in particular for keeping everything running smoothly (or at all) in the research group. I would also like send special thanks to my office mates over the years: Hannie, for the fun we had in the storage/office room during our master thesis; Emelie, for the moral support during the beginning of my PhD studies and in life in general; Antanas, for the board game tips and travel presents; and Johan, for keeping an unguarded chocolate box at the office.

I would also like to extend my infinite gratitude towards the MR personnel, especially those who has worked at Trion, for helping me with my data acquisition and for not laughing at me while I was attempting research. Thank you.

To my friends, Sara, Emil, Olof, Emma, Sanna, Johannes, and Leonora. Thank you for making bad times bearable and good times the best.

Lastly, I would like to thank my family, David and Nore. Thank you, David, for your unconditional and unwavering support and love, and for making me breakfast every day. Thank you, Nore, for being the funniest, most adorable and brilliant kid that ever existed (you know, objectively).

List of papers

This thesis is based on the following publications, referred to by their Roman numerals:

I **Trinh L**, Lind E, Peterson P, Svensson J, Olsson LE, Månsson S. High-Resolution MR Imaging of Muscular Fat Fraction - Comparison of Three T_2-Based Methods and Chemical Shift-Encoded Imaging. *Tomography : a journal for imaging research*. 2017;3(3):153-162

II **Trinh L**, Peterson P, Brorson H, Månsson S. Assessment of Subfascial Muscle/Water and Fat Accumulation in Lymphedema Patients Using Magnetic Resonance Imaging. *Lymphatic Research and Biology*. 2019;17(3):340-346

III **Trinh L**, Peterson P, Leander P, Brorson H, Månsson S. In vivo comparison of MRI- and MRS-based quantification of adipose tissue fatty acid composition against gas chromatography. *Magnetic Resonance in Medicine*. Accepted April 3, 2020.

IV **Trinh L**, Bennet L, Stenkula K, Olsson LE, Svensson J, Peterson P, Månsson S. Estimation of fatty acid composition using MRI in Iraqi and Swedish born healthy men. Manuscript

All papers are printed with the permission of the publishers.

Abbreviations

BMI	Body Mass Index
cl	Chain length
CT	Computed tomography
DXA	Dual-energy x-ray absorptiometry
FAC	Fatty Acid Composition
FF	Fat fraction
FID	Free induction decay
GC	Gas chromatography
GC-FID	Gas chromatography with flame ionizing detector
IDEAL	Iterative Decomposition of water and fat with Echo Asymmetry and Least-squares estimation
MR	Magnetic Resonance
MRI	Magnetic Resonance Imaging
MRS	Magnetic Resonance Spectroscopy
MUFA	Monounsaturated fatty acid
NASH	Non-alcoholic steatohepatitis
ndb	Number of double bonds
NLLS	Non-linear least squares
nmidb	Number of methylene-interrupted double bonds
PRESS	Point-resolved spectroscopy
PUFA	Polyunsaturated fatty acid
ROI	Region-of-interest
SFA	Saturated fatty acid
STEAM	Stimulated echo acquisition mode
TR	Repetition time
UFA	Unsaturated fatty acid
WHO	World Health Organization

1 Introduction

According to the World Health Organization (WHO), approximately 39% of the world's adult population was overweight (BMI ≥ 25 kg/m2) in 2016, of which about 13 % was obese (BMI ≥ 30 kg/m2) (1). Between 1975 and 2016, the prevalence of obesity almost tripled. Obesity increases the risk of developing diabetes, cardiovascular disease, musculoskeletal disorders, fatty liver, and cancer (2–8). Globally, overweight and obesity are associated with a larger number of deaths than underweight (1).

There are many factors which can cause excess accumulation of fat and adipose tissue. Some are associated with lifestyle and cultural factors, such as diet, physical activity, and socioeconomic status (9), while others are linked to genetics (10,11) or various diseases (12). The exact relationship between accumulated adipose tissue and the development of certain diseases is not yet fully understood, but studies suggests that the location in which the fat accumulates and the amount of stored fat are of importance (9,13).

Thus, with the increased prevalence of obesity and obesity-related diseases, the interest of assessing body fat and adipose tissue has increased. As a consequence, several methods for estimating fat have emerged over the years, including biopsy, dual-energy x-ray absorptiometry (DXA), and computed tomography (CT) (14,15). However, the currently most common method for fat measurements is magnetic resonance imaging (MRI) (16), a technique with several advantages compared to the alternatives. First, it does not involve ionizing radiation, making it superior in cases or studies that include children or repeated measurements (e.g. longitudinal studies). Secondly, the accessibility is relatively high as most modern clinics have access to MRI scanners.

Further, MRI-based methods offer the possibility to quantitatively estimate the fat accumulation in various body parts and organs such as the liver and skeletal muscle, without the need for invasive procedures such as biopsies. Although there are numerous ways to assess fat using MRI (17–19), the most common method, often referred to as water/fat imaging or chemical shift-encoded imaging, is based on the different resonance frequencies of water and fat in the presence of an external magnetic field (20–23). Although water/fat imaging is an established method and has been used for fat quantification of various locations *in vivo* (17), other approaches have been suggested (24–26).

In addition to the amount and location of adipose tissue, it has also been suggested that the fatty acid composition (FAC) might be linked to disease conditions such as cardiovascular disease (27), inflammation (28), non-alcoholic steatohepatitis (NASH) (29–31), and cancer (32,33). The gold standard technique for measuring FAC is gas chromatography (GC), an invasive method which requires a biopsy of the tissue of interest.

Recently, however, methods for quantifying the FAC of adipose tissue using magnetic resonance spectroscopy (MRS) and MRI have been introduced (34–37). While both the MR-based methods are non-invasive alternatives to GC, the MRI-based approach offers the additional advantage of spatial information without the need of multiple measurements. This can be of great importance when studying large adipose tissue depots or adipose tissue with heterogeneous FAC distribution (38–40). Since the MRI-based FAC quantification method is relatively new, some optimization work is still needed, as well as validation against an independent technique. Also, the method's feasibility in both research and clinical questions needs to be explored further.

In the first part of this thesis, a brief overview of adipose tissue and its relevance to health and various diseases will be given, followed by the theoretical background of the MR-based fat and FAC quantification methods. Further, some possible applications will be investigated. In the second part, the papers and manuscripts included in this thesis work can be found.

1.1 Aims

This thesis has the following aims:

1. To evaluate a T_2-based fat quantification method using different algorithms to enable fat content mapping with very high spatial resolution (**Paper I**).
2. To investigate the intermuscular and intramuscular fat accumulation in lymphedema using water/fat imaging (**Paper II**).
3. To compare and validate MR-based FAC quantification methods *in vivo* against an independent gold standard technique (**Papers III**).
4. To assess the FAC of visceral and subcutaneous adipose tissue using MRI and compare them in two groups with different cardiovascular disease risk profiles (**Paper IV**).

2 Human adipose tissue

In the human body, there are two types of adipose tissue: white and brown. Briefly, brown adipose tissue, while still present in adults, is primarily found in infants. In contrast to white adipose tissue with the main task of lipid storage, brown adipose tissue utilizes stored lipids to produce heat so that the body can maintain body temperature by non-shivering thermogenesis (41). Recently, a third type of adipose tissue has been introduced as beige (or brite) adipose tissue which can be described as something in between, or a mix of, brown and white adipose tissue (11,41). In this thesis, only white adipose tissue has been considered and studied. Thus, this chapter will briefly overview the anatomic, metabolic, and chemical properties of white adipose tissue only, as well as its impact on health and diseases. Through the rest of the thesis, adipose tissue will always refer to white adipose tissue.

2.1 Adipose tissue and fat depots

Adipose tissue consists of compactly organized adipocytes, supported by connective tissue. A large proportion of the adipocyte volume is occupied by a lipid droplet, and the size of the adipocyte can vary greatly depending on the lipid amount. Energy storage is not the only purpose of adipose tissue; it is also an endocrine organ where adipocytes produce hormones, peptides and molecules that impact metabolism and cardiovascular regulation. Studies have even suggested that adipose tissue itself is the source of many metabolic and cardiovascular risks associated with obesity (42).

Depending on where in the body fat accumulates, it can be categorized as either subcutaneous, visceral, or ectopic, which differs functionally and metabolically from each other (11,43). The location, in which fat can accumulate, is called a fat depot and affects the risk of developing various metabolic and cardiovascular diseases (44–46). For example, visceral adipose tissue and ectopic fat seem to have a greater clinical relevance than subcutaneous adipose tissue (47–49). There are many factors which might affect the distribution of the accumulated fat, such as aging, genetic basis, physical activity, and ethnicity (49–51). Ageing, for example, seems to reallocate fat from subcutaneous to ectopic and visceral depots (49,52).

Ectopic fat accumulation refers to the accumulation of fat within organs or body parts with a limited fat storage capacity and where, in normal conditions, a very

small amount of fat is present. Common organs and body parts which can accumulate fat include liver, skeletal muscle, and pancreas (51,53–56). In addition to the factors linked to *in vivo* fat distribution mentioned previously, there are several diseases which are associated with ectopic fat accumulation including fatty liver disease (57,58), insulin resistance (59–61), diabetes (46,61,62), cardiovascular disease (63), muscle disease (64), and cancer (6). Considering the large amount of people affected with these diseases, simple and practical methods for measuring ectopic fat accumulation is therefore of great interest.

While the ectopic fat is characterized by deposition in locations normally not intended for fat accumulation, the visceral and the subcutaneous depots (Figure 2.1) are designed for fat storage. However, there are numerous anatomic and metabolic differences between the two depots (42). For example, even though the subcutaneous depot holds approximately 80 % of the total body adipose tissue and the visceral depot only 5-20 %, depending on sex and age (52,65), visceral adipose tissue deposition has been associated to disease conditions (similar to ectopic fat accumulation) in a larger extent (65).

Moreover, even within subcutaneous adipose tissue, studies have shown that deep and superficial subcutaneous abdominal adipose tissue (Figure 2.1) have different properties (38,40,62,66) and that deep subcutaneous adipose tissue is more associated with disease development (62,67).

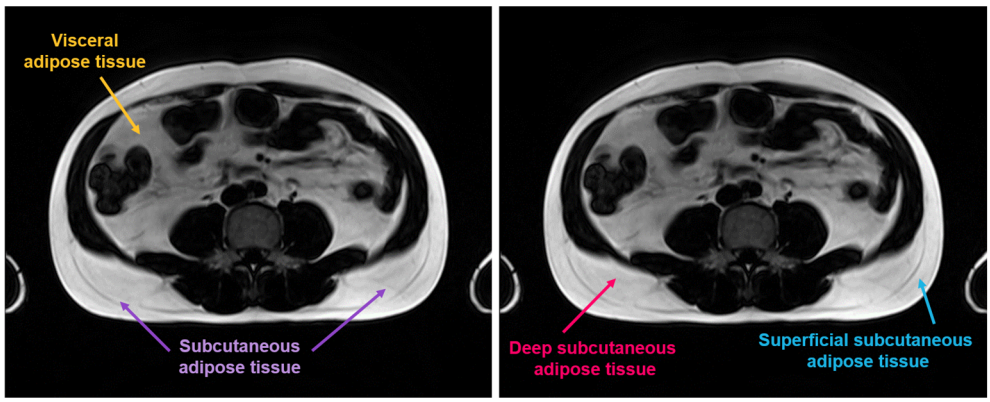

Figure 2.1 Visceral and abdominal subcutaneous adipose tissue of an axial MRI image. The deep and superficial subcutaneous adipose tissue, separated by Scarpa's fascia, are also indicated.

2.2 The triglyceride molecule and fatty acid composition

The main component of the lipid droplet stored in adipocytes is triglycerides (68). Triglycerides are esters which consist of three fatty acid chains connected to one glycerol back bone (Figure 2.2). There are different types of fatty acids and they can be characterized by the number of hydrocarbons and the type of bonds between them. Depending on the number of double bonds, the fatty acids can be described as saturated, unsaturated, monounsaturated, or polyunsaturated. Saturated fatty acids (SFA) have no double bonds, whereas unsaturated fatty acids (UFA) have at least one double bond. Further, unsaturated fatty acids can be either monounsaturated (one double bond, MUFA) or polyunsaturated (more than one double bond, PUFA). In addition to accumulation location and amount, adipose tissue can thus also be characterized by the proportions of SFA, UFA, MUFA, and PUFA.

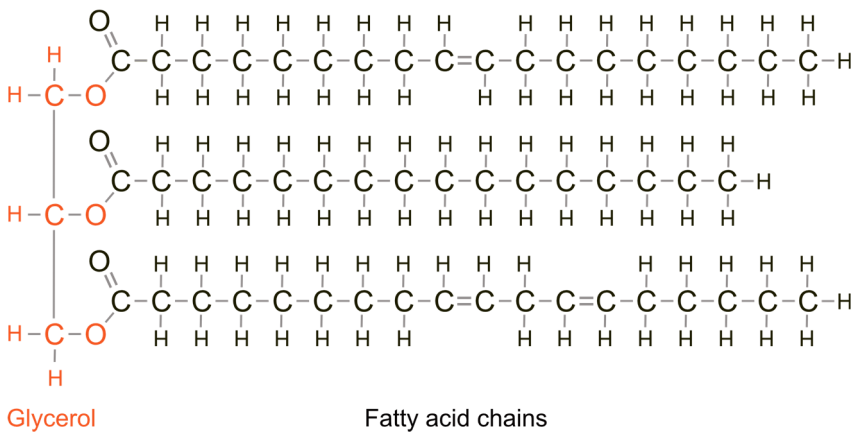

Figure 2.2 An example of a triglyceride molecule. On the glycerol back bone, three fatty acids are connected and depending on the number of double bonds (=), the fatty acid can be either saturated or unsaturated. Here, three types of fatty acids are presented: monounsaturated (top), saturated (middle), and polyunsaturated (bottom).

It has been reported that various adipose tissue compartments can have different fatty acid profiles (68). For example, visceral adipose tissue seems to have a larger proportion of SFA compared to subcutaneous adipose tissue (38), and a higher proportion of SFA in the deep subcutaneous adipose tissue compared to the superficial has been described (38,40,62). Differences in FAC of epicardial, pericardial, subcutaneous, and atrial adipose tissue have also been reported (27).

2.3 Fat accumulation and FAC in diseases

Excess fat deposition in skeletal muscle (3,69), liver (58,61), and pancreas (54) have been suggested to be associated with metabolic and cardiovascular diseases by previous studies (60,70). Fat deposition in skeletal muscle has shown to be important for estimating type 2 diabetes risk (3) but is also associated with several other diseases and syndromes (56,71,72). In skeletal muscle, fat can accumulate either in the intermuscular or the intramuscular compartment. Higher amounts of intermuscular adipose tissue can be found among patients with obesity and diabetes (69), and are associated with poor physical performance (73) and insulin resistance (69). Further, in the intramuscular compartment, fat can either be located in the intracellular or extracellular depot (74). High amounts of intracellular lipids have been related to both physical inactivity and high physical activity (74,75).

In **Paper II**, intra- and intermuscular far accumulation associated with lymphedema will be investigated further. Therefore, a short overview of fat accumulation in lymphedema patients will be given in *3.3 Water/fat imaging in lymphedema*.

Compared to fat and adipose tissue accumulation, the relationship between the FAC of adipose tissues and the risk of disease development has been less investigated. There has, however, been studies showing a significantly higher relative amount of liver SFA in patients with NASH than in those with simple steatosis (29,76,77). Similarly, higher levels of SFA has been found in the liver of patients with NAFLD (78) and of obese subjects (79), compared to controls. It has also been found that the FAC of bone marrow is associated with risk of fracture in diabetes patients (80), osteoporosis (81), and diabetes (82). Further, studies of breast cancer have suggested that lower amounts of UFA are associated with cancer compared to benign tumors (32,33,83).

In **Paper III** and **IV**, the FAC of adipose tissue were measured regarding the study of lymphedema (inflammation) and cardiovascular disease, respectively. Thus, short overviews of the role of FAC in lymphedema and inflammation, and cardiovascular disease will be given later (*4.8.1 Lymphedema* and *4.8.2 Hypertension and cardiovascular disease*, respectively).

2.4 The effect of dietary FAC on adipose tissue

The saturation and unsaturation degree of fat is commonly discussed when referring to dietary fat and oils such as butter, coconut oil (high on SFAs), olive oil (high on MUFAs), and fish oil (high on PUFAs), and their possible effects on the risk of developing obesity (84) as well as metabolic and cardiovascular disease (85–87) and inflammation (28). While some fatty acids are used directly after consumption,

others are stored in dedicated adipose tissue depots, such as subcutaneous adipose tissue, or transported by plasma and stored in organs, such as the liver. Adipose tissue has a half-life of 1-2 years and can therefore be used as a biomarker of dietary fat, reflecting the fatty acid intake over 2-3 years (68).

Correlation between the relative proportion of dietary and adipose tissue PUFA has been shown by several studies. In contrast, mixed results have been presented regarding the association between SFA and MUFA intake and adipose tissue FAC (68,88).

2.5 Measurement methods

2.5.1 Fat content

There are several methods for *in vivo* assessment of adipose tissue, from simple anthropometric measurements of body proportions, including waist circumference, and BMI, to more complex methods using various modalities. While some modalities are limited to assessing the adipose tissue volume in the subcutaneous and visceral depots only, for example DXA, ultrasound, and bioimpedance analysis, other approaches, such as CT and MRI, have the possibility to also estimate ectopic fat (14) and are considered to be the most accurate methods for *in vivo* fat estimation.

Though both CT and MRI are image-based methods, CT is less sensitive to breathing artefacts and might result in an easier segmentation of adipose and muscle tissue in skeletal muscle due to the use of Hounsfield unit values (15). However, MRI has a superior soft tissue contrast and does not expose the subjects to ionizing radiation. Over the years, MRI has become the most commonly used method for fat content quantification and can even be considered to be gold standard (19).

MRI offers a variety of different methods for assessing fat volume and content (17). One of those is water/fat imaging, a quantitative method which can be used to estimate fat content within an organ (e.g. liver or skeletal muscle) (53,89,90) as well as estimate subcutaneous and visceral adipose tissue volume (91). While this thesis will mainly focus on water/fat imaging (**Papers I** and **II**), an alternative MRI approach based on the different T_2-relaxation times of fat and water will be investigated as well (**Paper I**).

2.5.2 Fatty acid composition

In contrast to fat content measurements where there are many alternative methods, available methods for assessing FAC are limited. The gold standard technique for measuring FAC is GC. Briefly, GC allows for the analysis of mixtures by separating

them into their components. In the case of FAC analysis using GC, the triglycerides are first separated into fatty acids and glycerol, for example by hydrolysis and methylation. After that, the various fatty acids are separated from each other based on their different chemical properties. The relative abundance of each specific fatty acid can be then be measured using a detector. There are several different types of detectors which can be combined with GC, one of the most common ones for organic compounds are the flame ionizing detector (GC-FID) (92), which is sensitive to mass. After the biopsy samples have been through the process of GC, the separated fatty acids continue to the detector where the hydrocarbons are burnt by a flame, producing ions. The ions are then measured by electrodes and the amount of each fatty acid relative to the total amount of fatty acids, can then be obtained.

Although the method is useful in FAC quantification of e.g. dietary fats or oils, the invasive nature of retrieving human biopsy samples makes GC a less suitable method for studies requiring repeated measurements, such as longitudinal studies or studies of large heterogeneous tissues, studies of organs deep within the body, or large scale *in vivo* studies. As a consequence, studies of FAC of adipose tissue *in vivo* have been limited and non-invasive FAC quantification methods has been sought after.

As a non-invasive alternative to GC, MRS has been used for FAC quantification (34,40,93–95), and recently, also an MRI-based method has been introduced (35–37,96), based on an MRS approach suggested by Hamilton et al. (34). In addition to offering a non-invasive method for assessing adipose tissue FAC, MRI has the added possibility of obtaining spatial information without the need of excessive measurements.

In this work, FAC quantification methods using MRI (**Papers III** and **IV**) and MRS (**Paper III**), based on the approach suggested by Hamilton et al. (34), have been investigated and used. Detailed descriptions of the methods will therefore be given in the following chapters. The GC-FID was used as the reference method for FAC quantification in **Paper III**.

3 Fat quantification using MRI

There are numerous MRI-based techniques for separating fat and water (17). In this thesis, two different methods have been used: water/fat imaging (**Papers I** and **II**) and separation based on differences in T_2-relaxation time (**Paper I**). A theoretical outline of the two techniques will be given in this chapter. Water/fat imaging was used to study intermuscular and intramuscular fat accumulation (**Paper II**).

3.1 Water/fat imaging

Today, using MRI to quantify the fat content of various organs are considered the gold standard technique (19). One of the most commonly used methods, first introduced by Dixon (23), is based on the fact that water and fat precesses at different frequencies in a magnetic field. Thus, at given echo times, t_{IP} and t_{OP}, the water and fat signals, W and F, respectively, are either in-phase or opposed phase, respectively:

$$S(t_{IP}) = W + F \tag{3.1}$$

$$S(t_{OP}) = W - F. \tag{3.2}$$

By measuring the signal S at t_{IP} and t_{OP}, W and F can easily be solved for. However, Eqs. 3.1-3.2 do not consider the presence of B_0 field inhomogeneity ψ or T_2^*-relaxation time, both affecting the complex signal evolution over time. Moreover, this approach relies on a simplified expression of the fat signal since it only considers one fat resonance while, in reality, the MR fat signal consists of several resonances due to the more complicated molecule structure of triglyceride (Figure 2.2) compared to water. The use of several resonances is often referred to as a multi-peak model, opposed to using one single peak (the dominant fat peak, methylene) as a fat model.

To avoid bias from the above mentioned factors, an iterative method was suggested by Yu et al. (21) which estimates W, F, ψ, and T_2^* simultaneously, using multi-peak spectral modeling. The suggested approach, based on the Iterative Decomposition

of water and fat with Echo Asymmetry and Least-squares estimation (IDEAL) algorithm (20), uses the following complex signal model:

$$S(t) = \left(W + F \sum_{m}^{M} \alpha_m e^{i\omega_m t} \right) e^{\Psi t} \tag{3.3}$$

where α_m is the relative amplitude of fat resonance m, $\omega_m = 2\pi\Delta f_m$ and Δf_m is the chemical shift of fat resonance m relative to water, and $\Psi = i2\pi\psi - R_2^*$ is the complex field map (97). Converting the expressions to matrix form for N echoes, the signal model is then described by

$$\boldsymbol{S}_{N\times 1} = \boldsymbol{\Psi A \rho} \tag{3.4}$$

where

$$\boldsymbol{\Psi} = \mathrm{diag}\left(\mathrm{e}^{\Psi t_1}, \cdots, \mathrm{e}^{\Psi t_N}\right), \tag{3.5}$$

$$\boldsymbol{A} = \begin{bmatrix} 1 & \sum_{m}^{M} \alpha_m e^{i\omega_m t_1} \\ \vdots & \vdots \\ 1 & \sum_{m}^{M} \alpha_m e^{i\omega_m t_N} \end{bmatrix}, \tag{3.6}$$

and

$$\boldsymbol{\rho} = \begin{bmatrix} W \\ F \end{bmatrix}. \tag{3.7}$$

To solve for **ρ**, α_m and Δf_m are assumed to be known *a priori*. A detailed description of the algorithm steps is provided by Yu et al. (21).

Once the water and fat signal has been separated, the fat fraction *FF* can be calculated by

$$FF = \frac{F}{W + F} \tag{3.8}$$

voxel-by-voxel, creating *FF* maps (Figure 3.1).

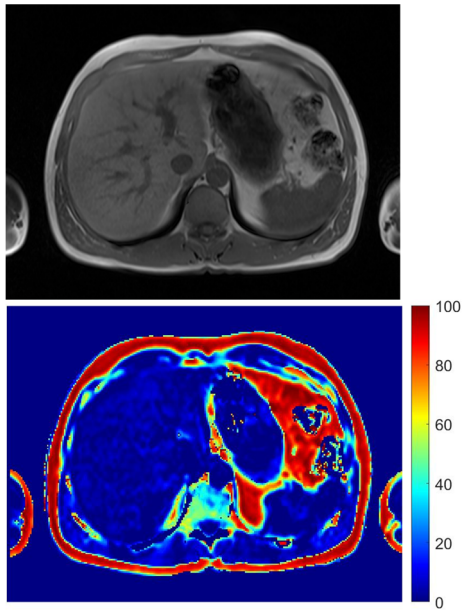

Figure 3.1 An MRI image of the liver (top) and the corresponding estimated *FF* map (bottom)

A limitation to the complex method described above is that the method is sensitive to phase errors caused by e.g. eddy currents. However, a complex approach is necessary to avoid the fat-water ambiguity at *FF* higher than 50 % associated with a magnitude-based method. Thus, a combination of the complex and the magnitude-based approaches has been suggested (98). Compared to the complex method, the hybrid method shows an improved robustness and better agreement to MRS results, especially at low fat fractions. In **Paper I**, the hybrid approach was used as low *FF*s were expected in a study of skeletal muscles of healthy volunteers and to minimize phase errors occurring due to inadequate combination of the acquired phase images from individual coil elements.

3.1.1 Acquisition strategies

Since the simple 2-point method was first suggested by Dixon, a few different Dixon-based methods have been introduced (99–102). Thus, there are several suggested ways to acquire MRI data for fat and water separation. Here, only the acquisition approach for the water/fat imaging method used in this thesis will be considered.

Usually, water/fat imaging is performed using multi-echo gradient echo images. Although the IDEAL-based methods are not restricted to certain echo-times, equidistant echoes with short inter-echo spacing are recommended. Usually, six

echoes are collected and used for quantitative imaging while fewer echoes are common for qualitative imaging (97,101).

Since the T_1-relaxation time of fat is shorter than that of water, the estimated FFs will be overestimated if the acquired images are T_1-weighted. To minimize the T_1-bias, it is recommended to use a small flip angle or a long repetition time (103).

3.2 T_2-based fat quantification

Although water/fat imaging is commonly used in both research and clinical applications, it is also limited in terms of spatial resolution. An increase of image resolution also increases the minimum possible inter-echo spacing, which in turn may impair the quantification accuracy of the method (104). A comparison of *FF* estimations using MR images with low (matrix size 128x128) and high (matrix size 512x512) spatial resolution is shown in Figure 3.2. High spatial resolution is valuable in heterogeneous tissues, such as skeletal muscle where studies of the different muscle groups or inter- and intramuscular adipose tissues are of interest (56,59,71,105–107).

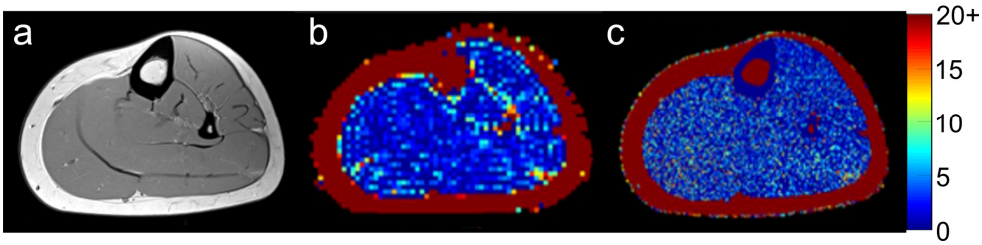

Figure 3.2 (a) An axial MRI image of a calf and the corresponding estimated *FF* maps using water/fat imaging with matrix size (b) 128x128 and (c) 512x512. While the resolution is too low in (b), the noise level in (c) is too high, concealing the anatomy of the muscles.

An alternative fat quantification method has been suggested previously (24,108), which instead of taking advantage of the different resonance frequencies of the fat and water signals uses the differences in T_2-relaxation times to separate fat and water. Therefore, a spin-echo sequence was used with a corresponding signal model described by

$$S(t) = We^{-\frac{t}{T2_W}} + Fe^{-\frac{t}{T2_F}} \tag{3.9}$$

where $T_{2,W}$ and $T_{2,F}$ are the T_2-relaxation times of water and fat, respectively.

In **Paper 1**, a T_2 method for quantification using high-resolution images was investigated and compared to water/fat imaging. Three different fitting algorithms were used for the T_2-based method and low resolution water/fat imaging was used as reference.

A 2-parameter and a 3-parameter fitting method were used and both approaches were based on Eq. 3.9. However, while the 2-parameter fit estimated *W* and *F* with fixed values of $T_{2,W}$ and $T_{2,F}$ known *a priori*, the 3-parameter fit estimated *W*, *F*, and $T_{2,W}$, and used a fixed value of $T_{2,F}$. The bi-exponential fits for estimation of *W*, *F* (and $T_{2,W}$) were carried out using simple linear regression and trust-region based NLLS algorithms in the 2-parameter and 3-parameter case, respectively.

Although NLLS is a commonly used fitting algorithm, it may have problems when the abundance of one component is far greater than the other (109,110). In the case of skeletal muscle, it can be expected that the fat signal is relatively low compared to the water signal. Therefore, also an alternative fitting method was considered. The third T_2-based method was based on Bayesian probability theory, similar to an approach previously suggested for intra-voxel incoherent motion imaging (111). The method will be briefly overviewed here.

For the Bayesian approach, a slightly different signal model was used:

$$S = S_0\left((1-f)e^{-\frac{t}{T_{2,W}}} + fe^{-\frac{t}{T_{2,F}}}\right), \tag{3.10}$$

where S_0 is the signal at $t = 0$ and f is the fat fraction. For a given S and prior information I, the joint posterior probability for $T_{2,W}$, $T_{2,F}$, and f can then be written as

$$P\left(T_{2,W}T_{2,F}f|SI\right) = \frac{P\left(S|T_{2,W}T_{2,F}f\right)\cdot P\left(T_{2,W}T_{2,F}f|I\right)}{P(S|I)} \tag{3.11}$$

where $P(S|I) = 1$ is the normalization factor, $P\left(T_{2,W}T_{2,F}f|I\right)$ is the joint prior probability of $T_{2,W}$, $T_{2,F}$, and f, given by the uniform distributions $U(0,0.06)$, $U(0.06,1)$, and $U(0,1)$, respectively. For the number of echoes N, the direct probability can then be described as

$$P\left(S|T_{2,W}T_{2,F}f\right) \propto \left[\frac{1}{2}\sum\left(S - S_0\left[(1-f)e^{-\frac{t}{T_{2,W}}} + fe^{-\frac{t}{T_{2,F}}}\right]\right)^2\right]^{-\frac{N}{2}}. \tag{3.12}$$

Using MATLAB's built-in function *slicesample* (Copyright 2005-2011 The MathWorks, Inc.)(112), $T_{2,W}$, $T_{2,F}$, and f, were estimated by slice sampling $P(T_{2,W}T_{2,F}f|SI)$. From f, $W = S_0(1-f)$ and $F = S_0 f$ could then be calculated.

Before the *FF* could be calculated using Eq. 3.8, possible T_1-relaxation bias needed to be considered. Due to the long T_1-relaxation time of muscle tissue (1420 ms at 3T (113)), the repetition time (TR) required to avoid T_1 bias was not clinically practical. Thus, T_1 corrections were carried out in the post-processing step using *a priori* T_1-relaxation times (113) rather than in the acquisition step.

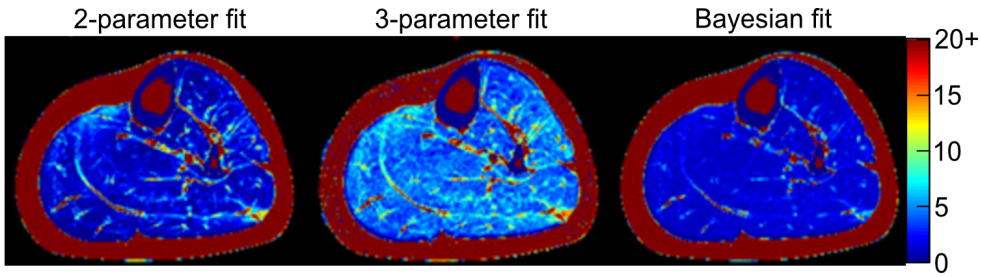

Figure 3.3 The estimated high resolution *FF* maps using a T_2-based method with three different fitting approaches (2-parameter, 3-parameter, and Bayesian fits). All three methods showed a superior anatomic depiction compared to high resolution water/fat imaging. However, the estimated *FF*s clearly differs between the T_2-based methods, suggesting that at least one of the methods will show poor agreement to the reference method (low resolution water/fat imaging).

All of the three fitting algorithms resulted in high resolution *FF* maps where anatomic information was clearly available (Figure 3.3). For example, the different muscle groups were clearly distinguishable and larger fat streaks visible. Of the fitting algorithms, the 2-parameter approach showed the best agreement to the reference method with high correlation within this range of *FF*s (Figure 3.4).

Although the T_2-based methods generated *FF* maps with superior anatomic information compared to high-resolution water/fat imaging (Figure 3.2), there are several drawbacks of the approach. One limitation arises if a tissue with a long T_1-relaxation time is present making a very long TR or a T_1-correction necessary. A T_1-correction might introduce bias due to uncertainties of the T_1 relaxation times, but using a long TR might not be practically realistic. Similar to the risk of bias due to incorrect T_1 relaxation times, another possible source of bias is the assumed $T_{2,F}$- and $T_{2,W}$-relaxation times used in the 2-parameter and 3-parameter approach. Other possible biases include the methods sensitivity to B1 field inhomogeneity and the presence of other compounds. No correction for B1 inhomogeneity was carried out in this work but a few different correction approaches have been suggested previously (25,26,114). Lastly, multi-echo spin echo sequences are associated with long acquisition times which may limit the method's applicability in larger study volumes.

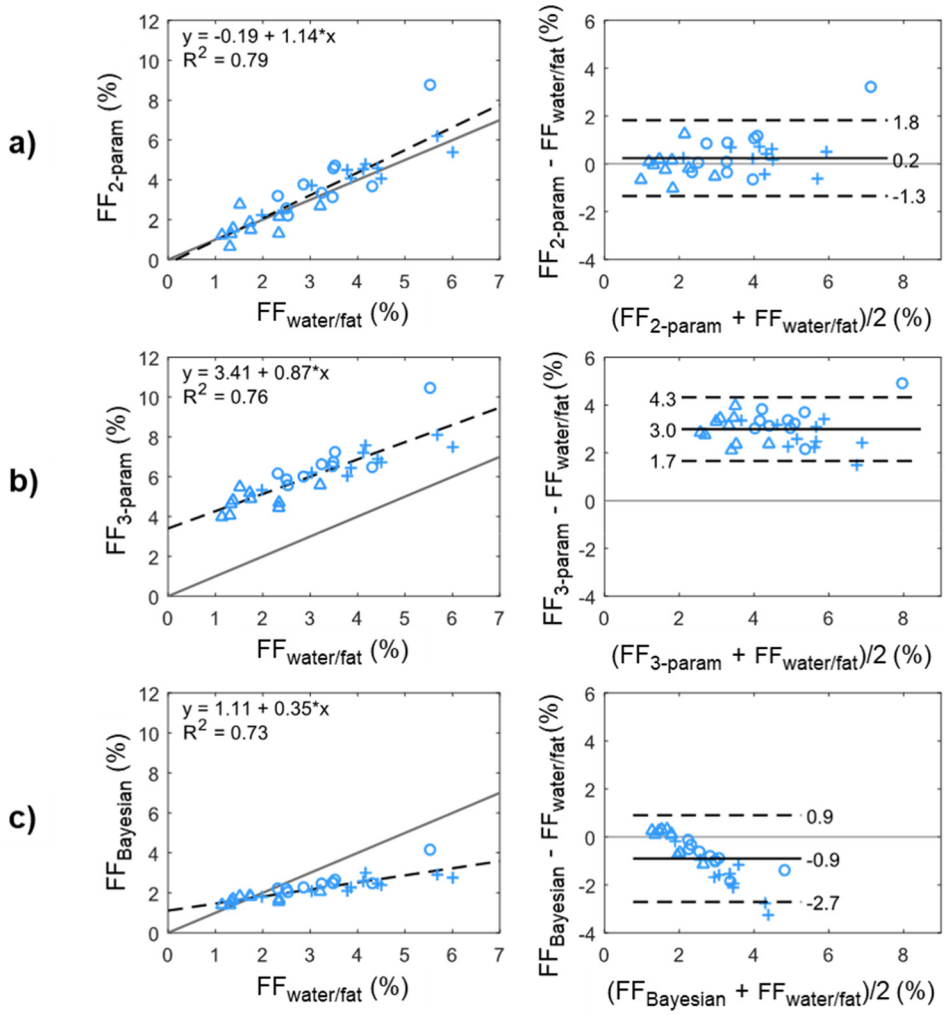

Figure 3.4 The linear regression and Bland-Altman plots for the (a) 2-parameter, (b) 3-parameter, and (c) Bayesian fitting methods compared to low resolution water/fat imaging (reference method). A good agreement between the 2-parameter fit was found while the *FF*s were overestimated using 3-parameter NLLS.

3.3 Water/fat imaging in lymphedema

Lymphedema is characterized by an insufficient lymph fluid drainage resulting in an accumulation of excess fluid and fat (115). It is a chronic disease and can either be caused by abnormalities in the development of the lymphatic system (primary lymphedema) or as a consequence of cancer treatment (such as radiation therapy and removal of lymph nodes), cancer, parasitic infections, or obesity (secondary lymphedema) (115–118). Lymphedema patients suffer from pain, swelling, restricted limb function, and a general decrease of life quality, and are prone to recurrent infections (115,119). Common treatment methods include the use of compression garments and liposuction (115,120,121).

The lymphatic system of the body can be separated into two systems: the superficial lymphatic system and the deep lymphatic system (122). The superficial lymph vessels run along the superficial venous system, collecting lymph from mainly the epifascial compartment. Similarly, the deep lymph vessels follow the deep venous system collecting lymph largely from the subfascial compartment. Thus, a disrupted lymphatic system might affect both the epifascial and the subfascial compartment of the limbs. Recently, it was shown that fat was accumulated in the subfascial as well as the epifascial compartment in lymphedema patients (91). While the excess accumulation of fat in the epifascial compartment has been investigated by several previous studies in lymphedema patients, the potential effects of lymphedema on the subfascial compartment is less investigated. Therefore, in **Paper II**, the fat accumulation of the subfascial compartment was investigated further using water/fat imaging.

The subfascial compartment was separated into an intermuscular and an intramuscular compartment (Figure 3.5). Both arm and leg lymphedema patients were included and the excess intermuscular and intramuscular fat volumes were studied at six time points: before liposuction (baseline), 4 days, 4 weeks, 3 months, 6 months, and 1 year after liposuction. A higher accumulation of fat was found in the intramuscular as well as the intermuscular compartment at almost all time points (Figure 3.6).

In addition, no correlations were found between the relative excess fat within either compartment and the relative excess epifascial adipose tissue or total limb volume (Figure 3.7). Further, no correlation between the relative excess intermuscular and intramuscular fat volumes was found (Figure 3.8). These results suggest that the intermuscular and intramuscular compartment needs to be studied separately and cannot be assessed through anthropometric measurements. Thus, water/fat imaging are able to contribute with unique knowledge in studies of subfascial fat accumulation.

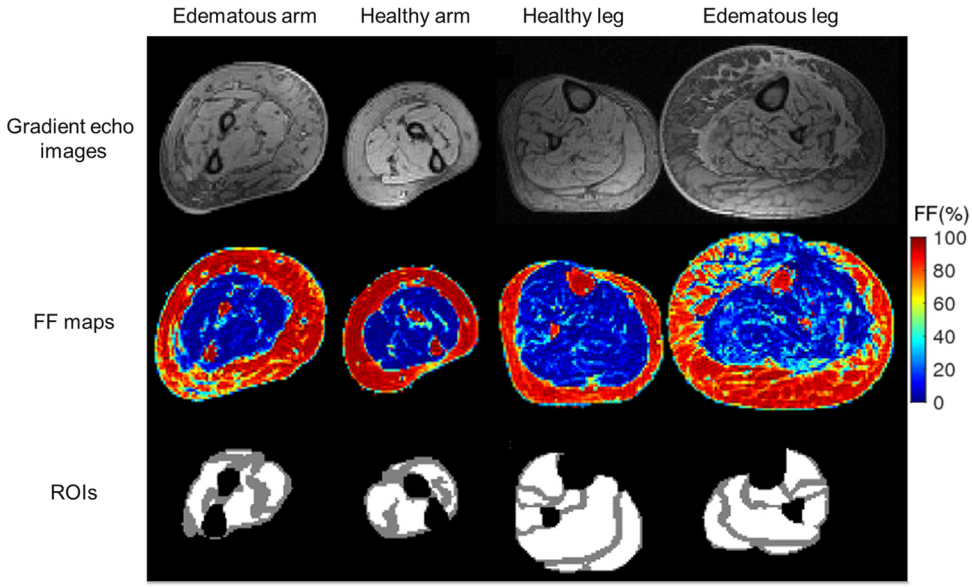

Figure 3.5 Examples of gradient echo images, estimated *FF* maps, and ROIs (intermuscular in gray and intramuscular in white) of a patient with arm lymphedema and a patient with leg lymphedema.

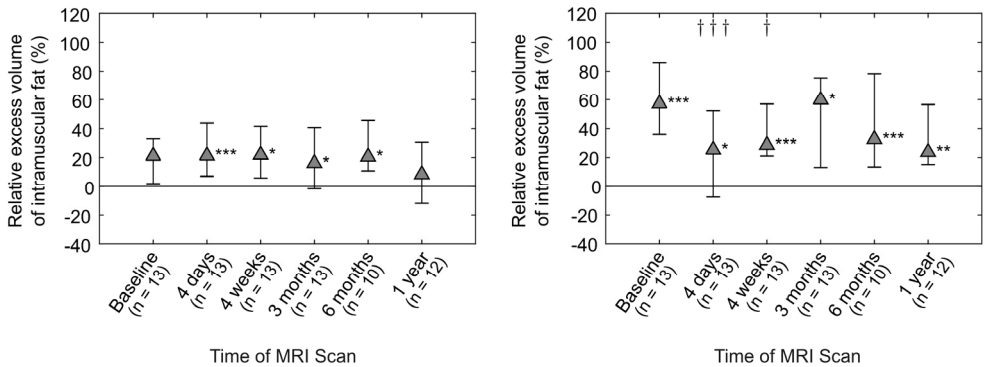

Figure 3.6 The median and first and third quartile of the relative excess volume of intramuscular and intermuscular fat at six time points. The relative excess fat volume was calculated as (fat edematous limb – fat healthy limb) / fat healthy limb. Higher amounts of fat were found in the edematous limb in both the intramuscular and intermuscular compartment, at all time-points. */**/*** denotes significant differences ($p < 0.05/0.01/0.001$) between the edematous and healthy limbs while †/††/††† represents the significant differences between baseline and the other time points.

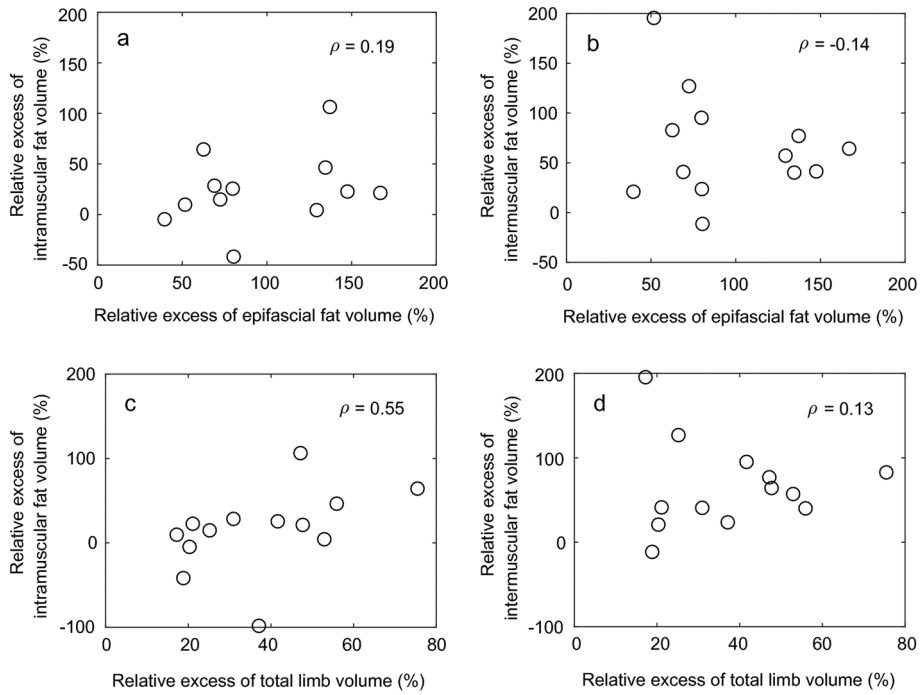

Figure 3.7 Comparisons between the relative excess of intramuscular fat and the (a) relative excess volume of epifascial fat and (c) relative excess of total limb volume. The corresponding comparisons with the relative excess of intermuscular fat are presented as well (b and d). No correlations were found (Spearman correlation coefficient ρ), indicating that independent measurements of intramuscular and intermuscular fat are needed.

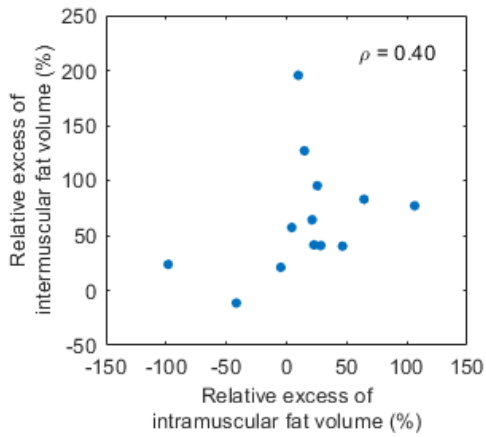

Figure 3.8 The relative excess of intermuscular compared to the relative excess intramuscular fat volume (%). No correlation was found (Spearman correlation coefficient ρ) between the two compartments, indicating that they need to be studied individually.

4 In vivo quantification of FAC using MR

Today, the gold standard technique for FAC measurements is GC of biopsy samples. However, the usefulness of the method for *in vivo* studies is limited due to its invasiveness. Since there are several studies suggesting that the FAC of adipose tissue might be associated with the risk of developing various diseases, as discussed previously (*2.3 Fat accumulation and FAC in diseases*), a less invasive approach is sought after.

In this thesis, different approaches of an MRS- and MRI-based method for fatty acid quantification have been investigated and compared to GC (**Paper III**). The methods will, therefore, be described in detail in this chapter. Furthermore, possible *in vivo* applications will be explored (**Papers III** and **IV**).

4.1 Definition of variables

To understand how the FAC can be estimated using MR, one must start with the triglyceride molecule and the MR signal associated with it. Due to the complex structure of the triglyceride molecule (Figure 2.2), it generates an MR signal which consists of several frequencies (Figure 4.1). Each frequency corresponds to a specific carbon-hydrogen constellation of the triglyceride molecule. Thus, by measuring the amplitude of each frequency, the abundance of the various carbon-hydrogen constellations can be assessed and the chemical composition of the fat estimated. This approach has previously been used to estimate adipose tissue FAC using MRS (93–95). However, a high enough spectral resolution is required to distinguish each peak of the spectrum. Using the field strengths commonly found in the clinic, this may not always be the case due to spectral overlap. Further, the approach is limited in the presence of a water signal as the water signal might conceal the fat peaks in close proximity.

Another way of describing the triglyceride molecule was introduced by Hamilton et al. (34). Instead of describing the triglyceride molecule by specific carbon-hydrogen constellations, it was described by the number of double bonds (*ndb*), the number of methylene-interrupted double bonds (*nmidb*), and chain length (*cl*). The MRS

peak amplitudes were then estimated through theoretical expressions based on *ndb*, *nmidb*, and *cl*, as shown in Table 4.1. Using this approach, the number of free parameters is reduced to three and spectra where each individual fat peak is distinguishable is no longer required.

While the estimation of *ndb*, *nmidb*, and *cl*, as described by Hamilton et al. (Table 4.1), was suggested for MRS applications, the approach was later adapted for MRI-methods (35–37) based on the same reconstruction algorithm as that for water/fat imaging. The theoretical details of both the MRS and MRI methods will be outlined in the following sections.

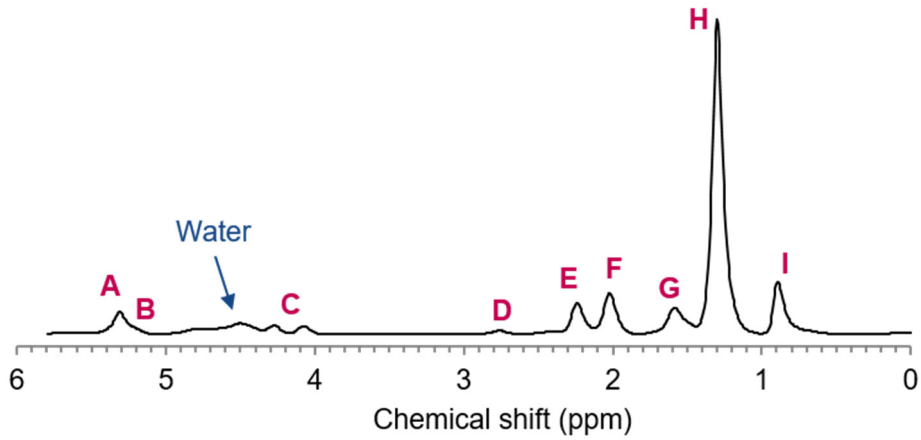

Figure 4.1 An MR spectrum of subcutaneous adipose tissue at 7 T. The amplitudes of peaks A-I are the signals corresponding to the triglyceride molecule.

Table 4.1 The fat peaks and their corresponding chemical shift and theoretical amplitudes suggested by Hamilton et al. (34). The peak denotations correspond to those in shown in Figure 4.1.

Peak (MRS)	Chemical shift (ppm)	Type	Assignment	Theoretical amplitudes
A	5.3	Olefin	-CH=CH-	2*ndb*
B	5.2	Glycerol	-CH-O-CO-	1
C	4.2	Glycerol	$-CH_2-O-CO-$	4
D	2.8	Diacyl	$-CH=CH-CH_2-CH=CH-$	2*nmidb*
E	2.2	a-Carboxyl	$-CO-CH_2-CH_2-$	6
F	2.0	a-Olefin	$-CH_2-CH=CH-CH_2-$	4(*ndb*-*nmidb*)
G	1.6	b-Carboxyl	$-CO-CH_2-CH_2-$	6
H	1.3	Methylene	$-(CH_2)_n-$	6(*cl*-4)-8*ndb*+2*nmidb*
I	0.9	Methyl	$-(CH_2)_n-CH_3$	9

4.2 Calculation of SFA, UFA, MUFA, and PUFA fraction

The chemical composition of fat is usually described by the relative amount of SFA, UFA, MUFA, and PUFA. Since *ndb* and *nmidb* are associated to the occurrence of double bonds and of multiple adjacent double bonds, respectively, they are clearly related to SFA, UFA, MUFA, and PUFA. However, it should be noted that the MR-estimated parameters *ndb*, *nmidb*, and *cl* refers to mean values per triglyceride and not per fatty acid. Hence, from the MR-estimated parameters *ndb* and *nmidb*, the fraction of UFA and SFA (f_{UFA} and f_{SFA}, respectively) can be calculated using the following expressions (36):

$$f_{UFA} = \frac{ndb - nmidb}{3} \tag{4.1}$$

and

$$f_{SFA} = 1 - f_{UFA}. \tag{4.2}$$

The fraction of MUFA and PUFA (f_{MUFA} and f_{PUFA}, respectively) can then be calculated as follows:

$$f_{MUFA} = \frac{ndb - 2nmidb}{3} \tag{4.3}$$

and

$$f_{PUFA} = \frac{nmidb}{3}. \tag{4.4}$$

For these expressions, it is assumed that the UFA is at most di-unsaturated, i.e. a fatty acid can only have a maximum of two double bonds. However, in reality, approximately 2-3% of adipose tissue fatty acids have more than two double bonds (93).

4.3 Models of *nmidb* and *cl*

To increase the robustness of the FAC quantification, it has been suggested to express *cl* and *nmidb* as functions of *ndb* to reduce the number of unknown parameters. Based on the empirical relationships between *ndb* and *cl*, and *ndb* and *nmidb*, found in a large range of mainly vegetable oils and fats, Bydder et al. (37)

suggested a quadratic expression for *nmidb*. Although the MRI-based approach for FAC quantification used in thesis is limited to linear expressions, a much wider range of possible *ndb* and *nmidb* values can be found among vegetable oils and fats compared to *in vivo*. Thus, within the range of values found *in vivo*, a linear expression is likely a good approximation.

Another expression of *nmidb*, based on reported GC analysis of the subcutaneous fat of ten healthy volunteers (94), has been suggested (123). Although an increased precision of the estimated *ndb* was found using the expression of *nmidb*, the GC data used to create the expression and the MRI-estimated values were obtained from different subjects. Thus, no comparison between GC and MRI or additional evaluation of the possible effects of using a constrained *nmidb* could be conducted. Further, due to low interpersonal variation, it has been suggested to use a fixed value of *cl* (123).

In **Paper III**, GC data from the subcutaneous adipose tissue of 18 lymphedema patients were acquired and used to create *in vivo* expressions for *nmidb* and *cl* as functions of *ndb*. By linear regression, the following relationships were obtained (Figure 4.2):

$$nmidb = 0.45ndb - 0.71 \tag{4.5}$$

and

$$cl = 0.38ndb + 16.32. \tag{4.6}$$

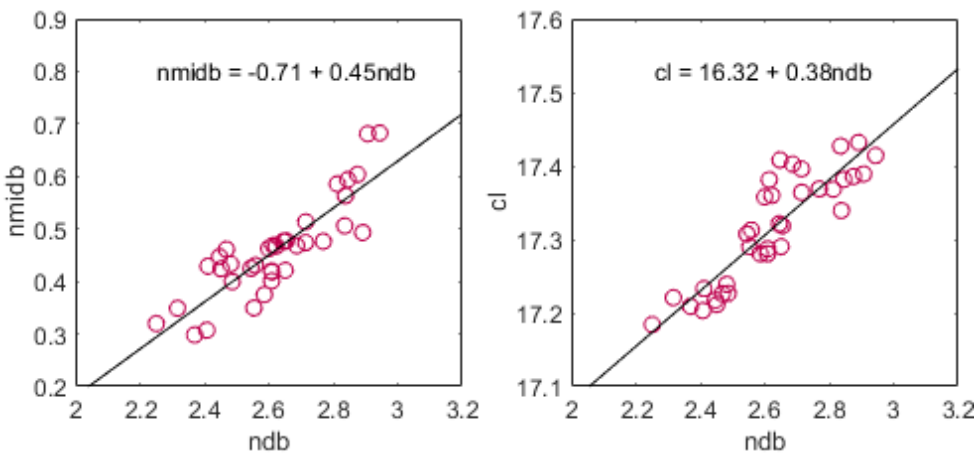

Figure 4.2 The expressions of *nmidb* and *cl* as functions of *ndb*, based on GC analysis of subcutaneous adipose tissue samples from the thighs.

Two different approaches have been evaluated in this thesis: a free and a constrained model. In the free model, *ndb* and *nmidb* were estimated as free parameters while *cl* was estimated using Eq. 4.6. Using the constrained model, only *ndb* was estimated as a free parameter while both *nmidb* and *cl* were estimated using Eq. 4.5 and Eq. 4.6, respectively. By combining Eq. 4.5 and Eq. 4.6, with the theoretical amplitudes presented in Table 4.1, new theoretical amplitudes can be obtained for the free and the constrained model, respectively (Table 4.2).

In **Paper III**, both the free and constrained models were investigated further, using both MRS and MRI. In **Paper IV**, the MRI-based method with the free model was used for FAC quantification subcutaneous and visceral adipose tissue.

Table 4.2 The fat peaks and their corresponding theoretical amplitudes depending on signal model. The amplitudes are modified versions of the ones introduced by Hamilton et al. (34) (the modified amplitudes are in bold) to include the expressions of nmidb and cl presented in Figure 4.2.

Peak group (MRS)	Theoretical amplitudes – free model	Theoretical amplitudes – constrained model
A	2*ndb*	2*ndb*
B	1	1
C	4	4
D	2*nmidb*	**0.896*ndb*-1.43**
E	6	6
F	4(*ndb*-*nmidb*)	**2.21*ndb*+2.87**
G	6	6
H	**73.9-5.73*ndb*+2*nmidb***	**72.5-4.84*ndb***
I	9	9

4.4 Quantification of FAC using MRS

4.4.1 Theory

The basic theory of MRS-based FAC quantification has already been outlined (see *4.1 Definition of the variables*). Using MRS, the free induction decay (FID) signal from a limited sample volume is acquired and Fourier transformed to enable a sorting of the MR signal per frequency (for an example, see Figure 4.1). Based on either the FID signal or the spectrum, the amplitude or area of each peak or resolvable peak cluster may then be estimated.

Using a NLLS fitting method, for example Levenberg-Marquardt, *ndb*, *nmidb*, and *cl* can be estimated from the theoretical expressions given in Table 4.1 or Table 4.2. However, before the parameters can be obtained, the peak amplitudes might need to be corrected for differences in T_2-relaxation between the various fat peaks,

depending on the used acquisition parameters. Although the different fat peaks have different T_2-relaxation times (44 - 80 ms at 3 T, measured in adipose tissue) (124), joint T_2-relaxation times for neighboring peaks might be necessary due to spectral overlap.

4.4.2 Acquisition strategies

Both stimulated echo acquisition mode (STEAM) (34,36,93,125,126) and point resolved spectroscopy (PRESS) (40,94,95) have been used for MRS-based FAC quantification. For T_2-correction, several spectra need to be acquired, each at a different echo time, from which separate T_2-relaxation times can be estimated or each peak or peak cluster.

Compared to STEAM, PRESS is more sensitive to J-coupling effects which can result in underestimations of T_2-relaxation times (127). Thus, STEAM might be considered the preferable alternative for FAC quantification (128,129), although it is important to note that J-coupling effects are present also using this sequence (130). To minimize the effect of J-coupling, short mixing time and echo times are desirable and long TR should be used to minimize T_1-weightning which may bias the estimations.

In **Paper III**, FAC quantification using MRS was conducted using T_2-corrected STEAM spectra.

4.5 Quantification of FAC using MRI

4.5.1 Theory

In contrast to MRS, MRI has the advantage of high resolution spatial information without the need of multiple measurements. Consequently, using MRI, it is possible to simultaneously estimate the FAC of different, large, or heterogeneous adipose tissue depots.

Recently, an MRI-based approach for FAC quantification was introduced (35,36), based on the theoretical amplitudes of the different fat peaks suggested by Hamilton et al. (34). The basic theory of this MRI-based FAC quantification method will be outlined in the following paragraphs. The assumed signal model can be described by

$$S(t) = \left(W + Ff \sum_{m}^{M} \alpha_m E_m(t) \right) e^{\Psi t} \tag{4.7}$$

where $f = 1/\sum \alpha_m$ is a normalization factor, α_m is the amplitude of the m:th fat peak as shown in Table 4.1, $E_m(t) = e^{i\omega_m t}$, and $\Psi = i2\pi\psi - R_2^*$ is the complex field map (97).

By combining Eq. 4.7 with the theoretical peak amplitudes given by Table 4.1, the signal model can be rearranged and expressed as

$$S(t) = \left(W + Ff(P_0 + P_1 ndb + P_2 nmidb + P_3 cl)\right) \mathrm{e}^{\Psi t} \tag{4.8}$$

where

$$\begin{aligned} P_0(t) &= E_1(t) + 4E_2(t) + 6E_4(t) + 6E_6(t) - 24E_7(t) + 9E_8(t) \\ P_1(t) &= 2E_1(t) + 4E_5(t) - 8E_7(t) \\ P_2(t) &= 2E_3(t) - 4E_5(t) + 2E_7(t) \\ P_3(t) &= 6E_7(t). \end{aligned} \tag{4.9}$$

The signal equation in matrix form for N echoes will then be

$$\boldsymbol{S}_{N\times 1} = \boldsymbol{\Psi A \rho} \tag{4.10}$$

where

$$\boldsymbol{\Psi} = \mathrm{diag}\left(\mathrm{e}^{\Psi t_1}, \cdots, \mathrm{e}^{\Psi t_N}\right), \tag{4.11}$$

$$\boldsymbol{A} = \begin{bmatrix} 1 & P_0(t_1) & P_1(t_1) & P_2(t_1) & P_3(t_1) \\ \vdots & \vdots & \vdots & \vdots & \vdots \\ 1 & P_0(t_N) & P_1(t_N) & P_2(t_N) & P_3(t_N) \end{bmatrix}, \tag{4.12}$$

and

$$\boldsymbol{\rho} = \begin{bmatrix} W \\ Ff \\ Ff \cdot ndb \\ Ff \cdot nmidb \\ Ff \cdot cl \end{bmatrix}. \tag{4.13}$$

Since **A** is known *a priori*, **Ψ** and **ρ** can be estimated iteratively as described previously (21,36), and maps of *FF*, *ndb*, *nmidb*, and *cl* may be reconstructed enabling simultaneous quantification of fat content and FAC (Figure 4.3).

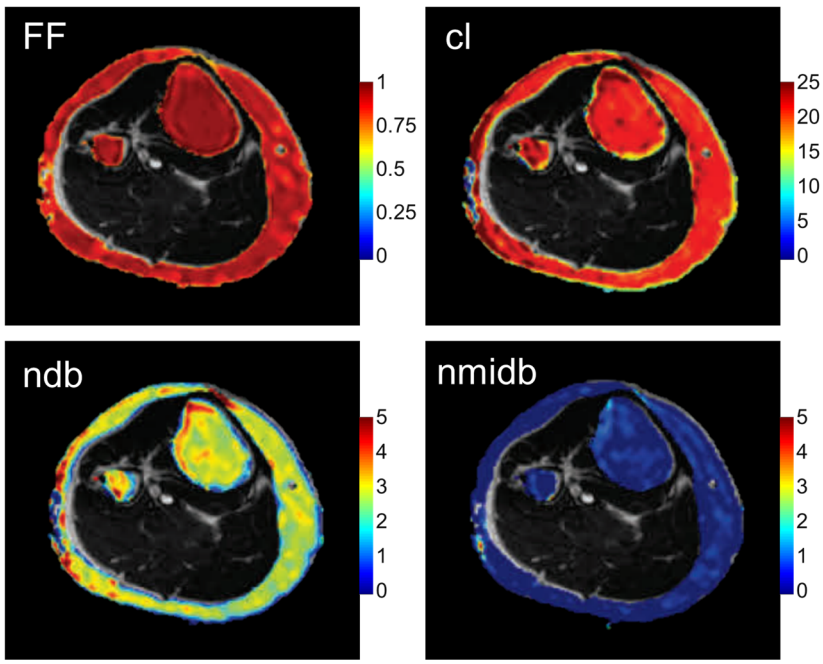

Figure 4.3 Examples of estimated *FF*, *ndb*, *nmidb*, and *cl* of subcutaneous adipose tissue and bone marrow of a calf, using the MRI-based FAC quantification method.

4.5.2 Adjusted signal expression

In this thesis, slightly modified versions of the approach described by Eq. 4.7-4.13 were implemented. Instead of estimating all of the FAC parameters based on the theoretical amplitudes given in Table 4.1, the theoretical amplitudes given in Table 4.2 have been used to reduce the number of estimates in an attempt to increase the robustness of the algorithm. Thus, Eq. 4.9 can be rewritten to

$$P_0(t) = E_1(t) + 4E_2(t) + 6E_4(t) + 6E_6 + 73.9E_7(t) + 9E_8(t)$$

$$P_1(t) = 2E_1(t) + 4E_5(t) - 5.7E_7(t) \qquad (4.14)$$

$$P_2(t) = 2E_3(t) - 4E_5(t) + 2E_7(t)$$

for the free model and

$$P_0(t) = E_1(t) + 4E_2(t) - 1.8E_3 + 6E_4(t) + 3.6E_5 + 6E_6 + 73.9E_7(t) + 9E_8(t) \quad (4.15)$$

$$P_1(t) = 2E_1(t) + E_3 + 4E_5(t) - 5.2E_7(t)$$

for the constrained model.

4.5.3 Acquisition strategies

Similar to water/fat imaging, FAC quantification using MRI is based on multi-echo gradient echo images with short inter-echo times. However, since there are a larger number of unknown parameters in the FAC estimation, additional echoes are required compared to water/fat imaging. A few studies have investigated the optimal acquisition settings and what effects various acquisition parameters might have on the estimated parameters. Only acquisition at 3 T will be considered here.

While the time of the first echo seems less important, it has been recommended to keep the inter-echo spacing shorter than 1.8 ms and the total read-out time longer than 15 ms (35). Using an inter-echo spacing smaller than 1.8 ms corresponds well with the results of Peterson et al. (36), where a noise analysis showed an unfavorable echo spacing at 2.2 ms. Another study found that for bipolar acquisition, the optimal total read-out time is around 14-18 ms for inter-echo times between 0.84 ms and 1.23 ms (131). Interleaved (37) or bipolar (131) acquisition might be alternatives to shorten the inter-echo spacing further. However, the majority of the published studies have used unipolar (flyback) acquisitions (35,36,39,77,96,126). In **Papers III** and **IV**, unipolar flyback gradients were used.

In contrast to water/fat imaging, T_1 weighting does not seem to affect the estimation of FAC (132). Therefore, a larger flip angle compared to water/fat imaging can be used to increase SNR. It should be noted, however, that if simultaneous estimation of fat content and FAC is of interest, T_1 relaxation effects must again be considered. In **Paper III**, the FAC of adipose tissue was estimated, therefore, the *FF* was not of interest and a relatively large flip angle (30 degrees) was used.

4.6 Comparison to GC analysis

The MR-based methods described in this thesis have been investigated previously with promising results (34–36,96,126,131). However, as the methods mainly have been validated in vegetable fats and oils (using GC or values obtained from the Swedish National Food Administration or manufacturer) or *in vivo* against MRS in

the MRI-case (34–37,96,125,126,131), further *in vivo* validation against independent methods is needed.

In **Paper III**, an *in vivo* comparison of the MRS and MRI-based methods against GC-FID was made. Biopsy samples of the medial subcutaneous adipose tissue and MR spectra and images were acquired 20 cm above the femoral condyles from 18 subjects (36 biopsies in total, one sample from each thigh). Both the free and the constrained model were investigated using both the MRS and the MRI approach.

4.6.1 MRS vs GC

For the free model, the MRS-estimated *ndb* and *nmidb* were both overestimated compared to GC-FID (Figure 4.4). A higher correlation was found between ndb_{MRS} and ndb_{GC} than between $nmidb_{MRS}$ and $nmidb_{GC}$. Comparing instead the MRS-estimated f_{SFA}, f_{MUFA}, and f_{PUFA} to GC (Figure 4.5), the highest correlation was found for f_{SFA} although it was underestimated. While the methods showed the best agreement for f_{MUFA}, the correlation was lower.

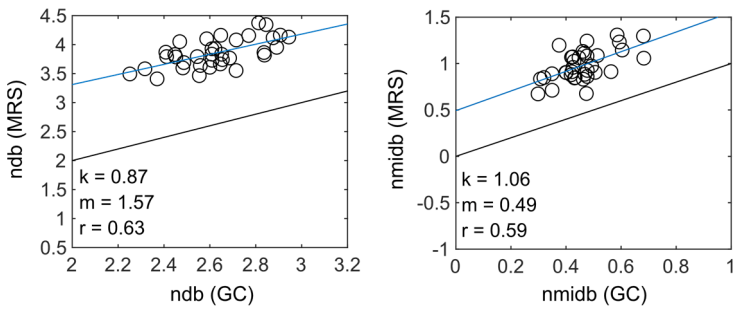

Figure 4.4 The estimated *ndb* (left) and *nmidb* (right) using MRS, compared to GC. The black lines are the identity lines and the blue lines represent the linear fits. A higher correlation (r) was found between the MRS-based method and GC in the estimation of *ndb* compared to the *nmidb* case. However, both *ndb* and *nmidb* are overestimated by MRS.

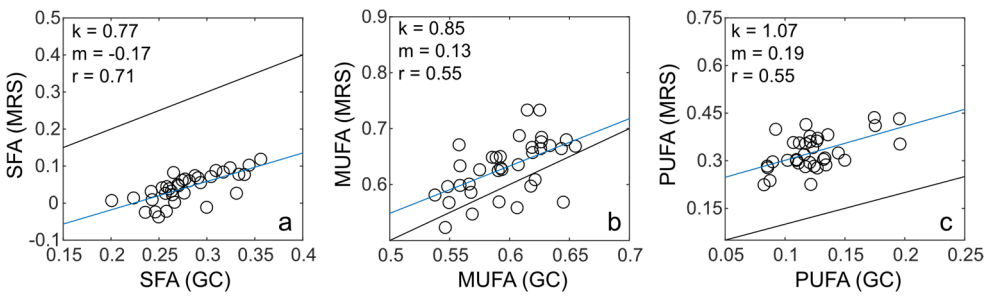

Figure 4.5 The estimated (a) f_{SFA}, (b) f_{MUFA}, and (c) f_{PUFA} using MRS, compared to GC. The black lines are the identity lines and the blue lines represent the linear fits. A higher correlation (r) between the MRS-based method and GC in the estimation of f_{SFA} compared to f_{MUFA} and f_{PUFA}. In contrast to the other estimated parameters, including *ndb* and *nmidb*, f_{SFA} was underestimated.

Using instead the constrained model for estimation of *ndb* and *nmidb*, similar agreements but higher correlations between the methods were found compared to using the free model (Figure 4.6). However, the effect of using a constrained model on the estimation of f_{SFA}, f_{MUFA}, and f_{PUFA} varied between the parameters (Figure 4.7). While the estimation of f_{PUFA} seemed to be improved by the use of the constrained model, the estimations of both f_{SFA} and f_{MUFA} resulted in lower correlations. Especially the estimation of f_{MUFA} was effected as no clear association to GC could be found. Instead, a nearly constant value of f_{MUFA} was obtained.

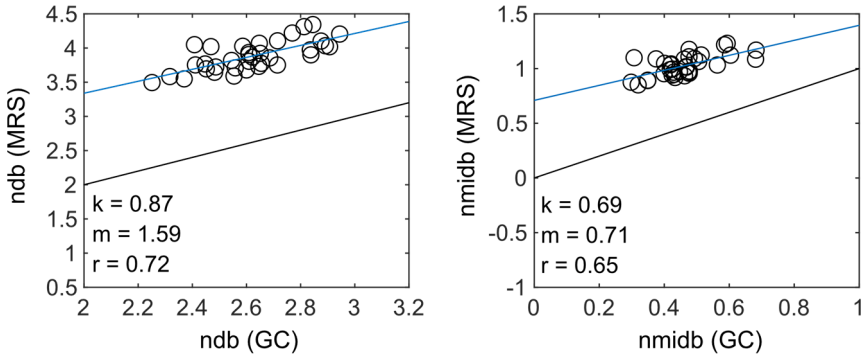

Figure 4.6 The estimated *ndb* (left) and *nmidb* (right) using MRS, compared to GC. The black lines are the identity lines and the blue lines represent the linear fits. Compared to using the free model, higher correlations between MRS and GC were found for both *ndb* and *nmidb*. However, *ndb* and *nmidb* are still overestimated by MRS.

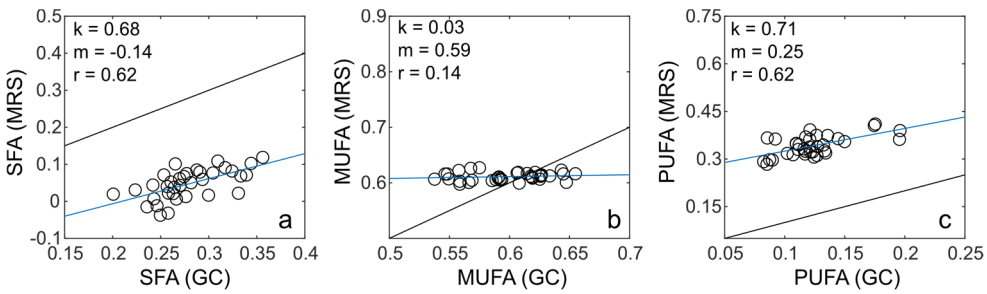

Figure 4.7 The estimated (a) f_{SFA}, (b) f_{MUFA}, and (c) f_{PUFA} using MRS, compared to GC. The black lines are the identity lines and the blue lines represents the linear fits. A higher correlation (r) between the MRS-based method and GC in the estimation of f_{SFA} compared to f_{MUFA} and f_{PUFA}. In contrast to the other estimated parameters, including *ndb* and *nmidb*, f_{SFA} was underestimated. Using the constrained model, an almost constant value of f_{MUFA} was estimated suggesting that the model is limited in terms of correctly separating MUFA and PUFA.

4.6.2 MRI vs GC

Using the free model, high correlations were found between MRI and GC for both *ndb* and *nmidb* (Figure 4.8), although both parameters were underestimated. Especially the MRI-assessed *nmidb* which was underestimated by almost 50% compared to GC.

In the case of f_{SFA}, f_{MUFA}, and f_{PUFA} (Figure 4.9), better agreements were found in general between the two methods. It seems as the systematic bias found in the estimations of *ndb* and *nmidb* are partly cancelled out in the calculation of f_{SFA} and f_{MUFA}. Although, a slight overestimation of f_{SFA} and f_{MUFA} and an underestimation of f_{PUFA} were still found. High correlations were found for all the parameters, albeit not as high as for *ndb* and *nmidb*.

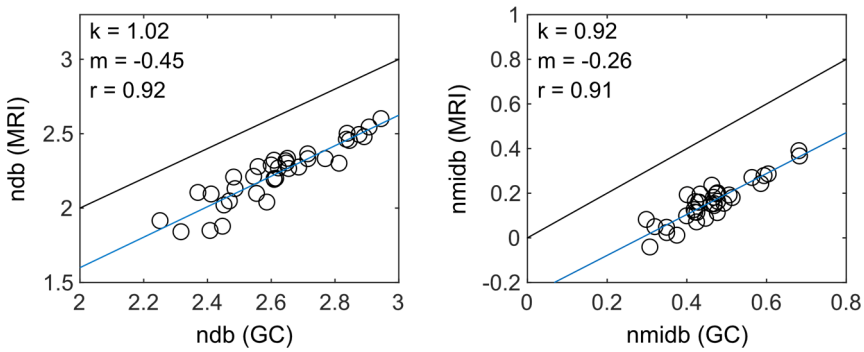

Figure 4.8 The estimated *ndb* (left) and *nmidb* (right) using MRI (free model), compared to GC. The black lines are the identity lines and the blue lines represent the linear fits. High correlations (r) can be found between the MRI-estimated parameters and GC. However, both *ndb* and *nmidb* are underestimated by the MRI-based approach.

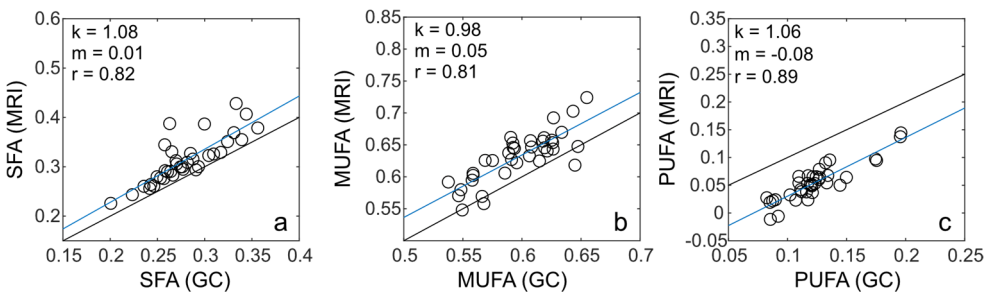

Figure 4.9 The estimated (a) f_{SFA}, (b) f_{MUFA}, and (c) f_{PUFA} using MRI (free model), compared to GC. The black lines are the identity lines and the blue lines represent the linear fits. High correlations (r) can be found between the MRI-estimated parameters and GC, albeit lower compared to the *ndb* and *nmidb* cases. While f_{SFA} and f_{MUFA} are slightly overestimated, f_{PUFA} is underestimated.

Compared to the free model, a slightly better agreement and a similar correlation were found between the constrained model and GC in the estimation of *ndb* (Figure 4.10). In the case of *nmidb*, a better agreement but worse correlation was found. Correspondingly, similar agreement and correlation were found for f_{SFA} while a better agreement but a worse correlation was found in the estimation of f_{PUFA}. A much worse correlation and an almost constant value of f_{MUFA} was found using the constrained model. This effect on f_{MUFA} was seen in the MRS-based method as well, suggesting that the constrained model limits the methods' ability to correctly separate MUFA and PUFA.

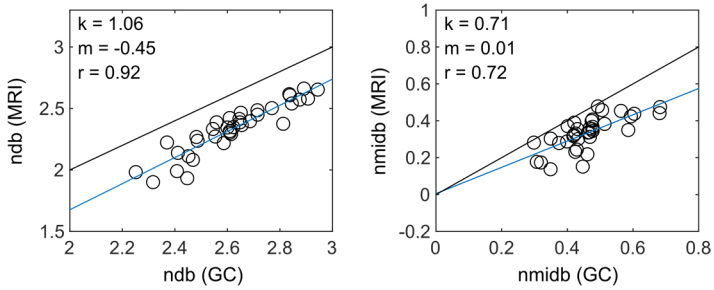

Figure 4.10 The estimated *ndb* (left) and *nmidb* (right) using MRI (constrained model), compared to GC. The black lines are the identity lines and the blue lines represent the linear fits. High correlations (r) can be found between the MRI-estimated parameters and GC. Compared to the free model MRI, similar estimation of *ndb* was obtained, although a slightly better agreement was found. While a better agreement was found for the *nmidb* case, a worse correlation was obtained here.

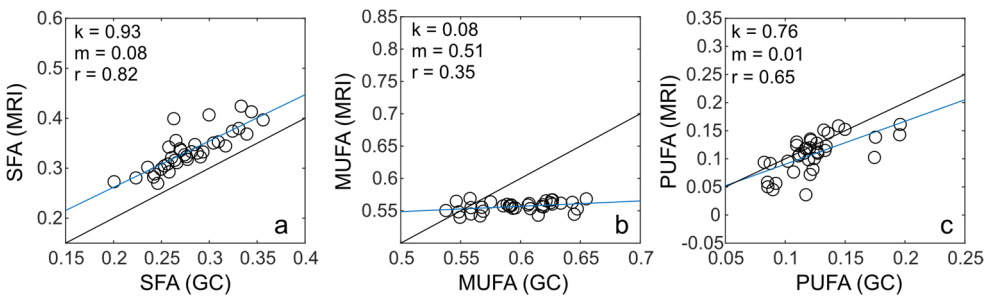

Figure 4.11 The estimated (a) f_{SFA}, (b) f_{MUFA}, and (c) f_{PUFA} using MRI (constrained model), compared to GC. The black lines are the identity lines and the blue lines represent the linear fits. High correlations (r) can be found between the MRI-estimated parameters and GC, albeit lower compared to the *ndb* and *nmidb* cases. While similar results for f_{SFA} was obtained here as in the free model case, the estimation of f_{MUFA} showed very low correlation to GC using the constrained model.

Examples of the estimated f_{SFA}, f_{MUFA}, and f_{PUFA} maps using the free and constrained models are depicted in Figure 4.12. The estimated f_{MUFA} map using the constrained model resulted in a very homogeneous map compared to the free model, reflecting the results in Figure 4.11.

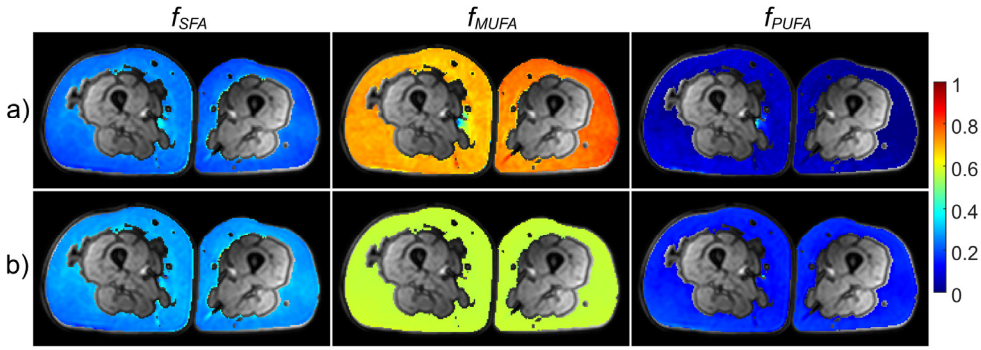

Figure 4.12 Examples of estimated f_{SFA}, f_{MUFA}, and f_{PUFA} maps using the (a) free and (b) constrained model.

4.6.3 Sources of bias

Some of the discrepancy between the MR-based methods and GC can be explained by the assumption that the triglycerides are at most diunsaturated in the MR cases. However, the bias is expected to be small as the relative amount of PUFA with higher unsaturation degree than two was low (1.8 % in average (Paper III), 2-3 % reported previously (93)). Further, fatty acids from phospholipids are included in the estimation of FAC using GC but not in the estimation using MRS or MRI since phospholipids are MR invisible. However, in adipose tissue, this particular bias is expected to be small.

By using the model for *nmidb* obtained from the GC data, the method's ability to correctly estimate f_{MUFA} and f_{PUFA} was negatively affected. The model assumes that a simple linear relationship exists between *ndb* and *nmidb*. However, this may not be the case. For example, when *nmidb* = 0, *ndb* can either be 0 or 1, i.e. saturated or monounsaturated.

In addition, in the MRS-case, the effect of J-coupling on the estimated T_2-relaxation times, and consequently the estimated T_2-corrected peak amplitudes and FAC parameters, cannot be disregarded.

4.7 Comparing MRS and MRI

Several studies have compared the MRS- and MRI-based FAC quantification methods with good agreement both in oil phantoms and *in vivo* (36,39,126). In contrast, low correlation and poor agreement were found between the MRS- and MRI-based methods described in this work (Figure 4.13). While there are several methodological differences between the two approaches which could explain the poor association, one plausible difference is due to the impact of J-coupling on the MRS estimation mentioned in the previous section (*4.6.3 Sources of bias*).

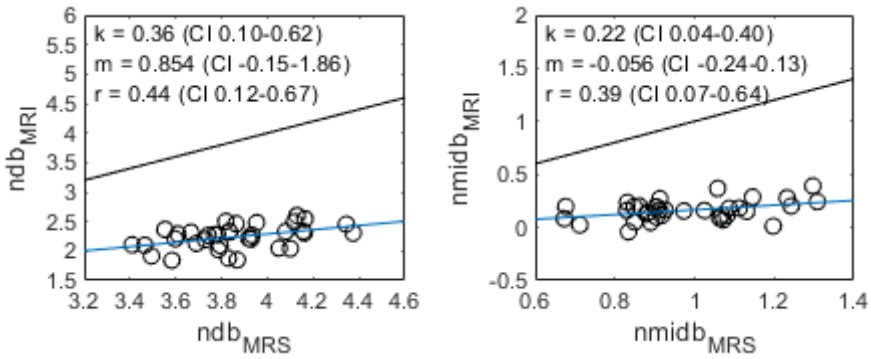

Figure 4.13 Comparison of the estimated *ndb* (left) and *nmidb* (right) using the MRI and the MRS-based method (free model). Low correlations and poor agreement were found between the methods in the estimation of both *ndb* and *nmidb*,

Further, there are numerous factors which may explain the different results in terms of the agreement and correlation between MRS and MRI presented here and in previous studies. Firstly, the used signal models and algorithms varies between the studies (especially for MRS). Also, in the *in vivo* cases, the investigated adipose tissue depots and body parts are different. Lastly, the MRS-based approach can be operator dependent in the analysis and post-processing steps.

4.8 Applications of MR-based FAC quantification

4.8.1 Lymphedema

In addition to excess accumulation of fat and fluid (see *3.3 Water/fat imaging in Lymphedema*), lymphedema has also been linked to chronic inflammation (133) and studies have suggested that inflammation and fat accumulation might be closely associated (134). Further, chronic inflammation may be associated to adipose tissue FAC (70,135). For example, an animal study has found that chronic inflammation alters the chemical composition of the adipose tissue intermediate to the lymph nodes (136,137). However, the association between the development of lymphedema and the adipose tissue FAC of the affected limb has not yet been investigated

In **Paper III**, the FAC of the subcutaneous adipose tissue of edematous thighs were assessed and compared to the corresponding parameters in healthy thighs using GC-FID, MRI, and MRS. In total, 19 lymphedema patients were included of which all underwent MR scans and 18 underwent biopsy sampling for GC-FID. The f_{SFA},

f_{MUFA}, and f_{PUFA} were assessed using the MRI and MRS approaches with a free model described previously.

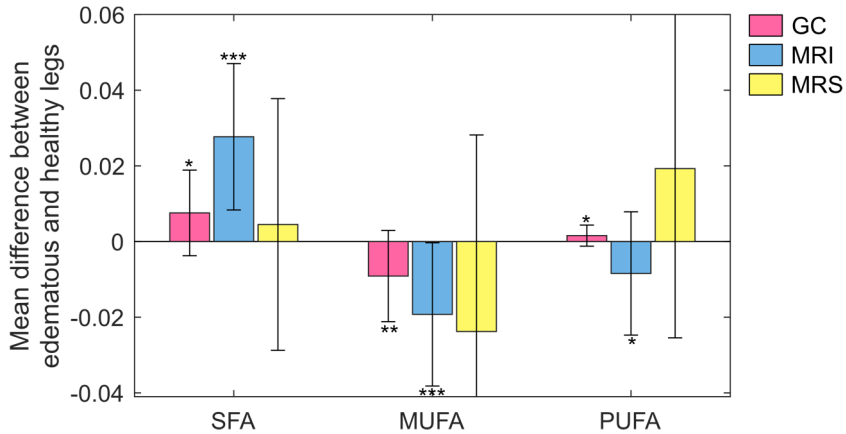

Figure 4.14 The mean differences (edematous - healthy) and standard deviation of the relative amount of SFA, MUFA, and PUFA, estimated using GC, MRI, and MRS. Significantly higher relative amount of SFA and PUFA were found in the edematous thigh with GC analysis, Similar results were found using the MRI-based method, although with greater differences and higher proportion PUFA in the healthy thigh. No significant differences were found with the MRS. */**/*** denotes p-values < 0.05/0.01/0.001.

Significant differences ($p < 0.05$) were found between the edematous and healthy thighs (edematous - healthy) using GC and MRI (Figure 4.14). Using GC, higher relative amounts of SFA and PUFA were found the edematous thigh. Although further investigation of the underlying reason for the FAC differences were out of the scope of **Paper III**, the results suggest that the FAC of adipose tissue might be on interest in the quest of fully understanding the development and consequences of lymphedema.

Here, the differences estimated with GC-FID analysis are considered to reflect the true differences in FAC between the edematous and healthy thigh. While large standard deviations and no significant differences were found using MRS, the MRI-based approach found similar results as GC but the differences were larger between the thighs. One possible explanation for this is the, probably artefactual, spatial variation over the estimated maps (see Figure 4.12) (37). To minimize the effect on the results, the MRI values were calculated using smaller ROIs which were placed in the medial area of the subcutaneous adipose tissue. However, bias due to the spatial variation cannot be entirely discarded.

4.8.2 Hypertension and cardiovascular disease

In a previous study, higher prevalence of hyperlipidemia, insulin resistance, and diabetes type 2, but a lower prevalence of hypertension was found among a Iraqi-born population in Sweden compared to a Swedish-born population (138). As both diabetes type 2 and hypertension normally are highly associated with cardiovascular disease (139), it was suggested that the risk profile for cardiovascular disease of the Iraqi-born subjects might differ from that of Swedish-born (138).

Although the underlying reason for the difference in hypertension prevalence between the Iraqi-born and Swedish-born group is unknown, it has been hypothesized that it might be related to differences in diet (140). In general, the association between cardiovascular disease and hypertension and dietary FAC has been ambiguous (87,141,142). However, studies have suggested that excessive consumption of SFA is linked to elevated risk for cardiovascular disease (87) and that replacing SFA with MUFA can have a positive effect on blood pressure (143). It has also been suggested that high MUFA diet improves the cardiovascular disease risk factors compared to low MUFA diets (144) as well as decreases plasma triglycerides and blood pressure (142,145). In the case of PUFA, studies suggest a positive effect on cardiovascular health, however, similarly to SFA and MUFA, the reported effects have varied (87,146).

To study the possible relationships between dietary FAC and cardiovascular health, food questionnaires can be used. However, self-reported dietary intake methods are prone to errors due to recall bias and misreporting (147,148). Another approach is measuring the fatty acids of plasma or adipose tissue as biomarkers of dietary intake. While plasma fatty acids mainly reflect the dietary intake over a few hours-days, the FAC of adipose tissue reflects the dietary intake the over weeks-months (147), or even years (68). However, there are some limitations with using biomarker of dietary intake. For example, in addition to diet, factors such as genetics, physical activity, smoking, and alcohol consumption may also have an impact on adipose tissue FAC (88). Thus, the FAC of adipose tissue reflects a far more complex measure than solely fatty acid consumption. While correlation between dietary and adipose tissue PUFA has been found, mixed results have been presented regarding the association between SFA and MUFA intake and adipose tissue FAC (68).

In **Paper IV**, the FAC in adipose tissue of 14 Swedish-born and 23 Iraqi-born healthy men in Sweden were estimated and compared using the MRI-based FAC quantification method (Figure 4.15). Due to the different metabolic roles of subcutaneous and visceral adipose tissue, the two depots were studied separately.

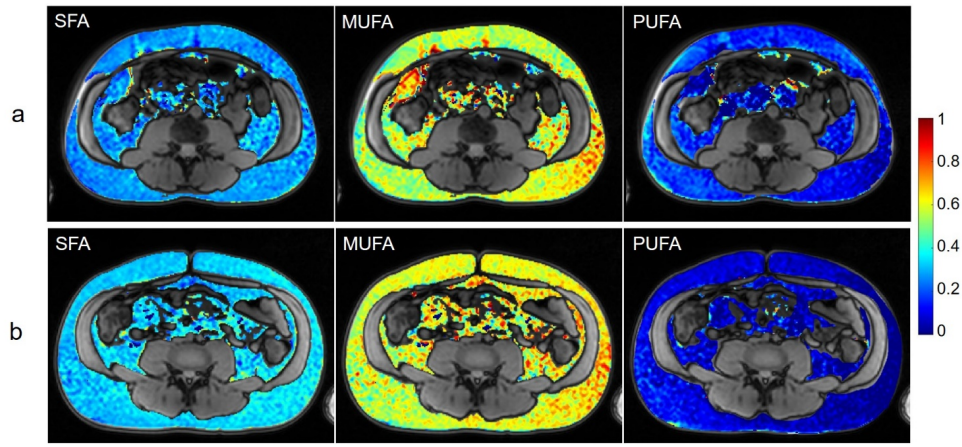

Figure 4.15 Example SFA, MUFA, and PUFA maps of two subjects representing the a) Iraqi-born and b) Swedish-born men.

The mean estimated f_{SFA}, f_{MUFA}, and f_{PUFA} are shown in Figure 4.16. Significantly lower f_{SFA} and f_{MUFA}, and significantly higher f_{PUFA} were found in the subcutaneous adipose tissue of the Iraqi-born men compared to the Swedish-born men (Table 4.3). Similar differences were found in the visceral depot, except that the difference in f_{MUFA} was not significant. Comparing instead the FAC of the subcutaneous and visceral adipose tissues (subcutaneous - visceral), significant differences in both f_{MUFA} and f_{PUFA} were found among the Iraqi-born while a significant difference in f_{MUFA} was found Swedish-born men (Figure 4.17).

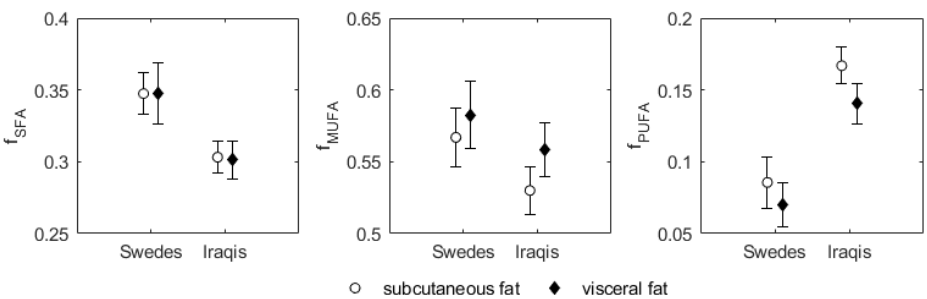

Figure 4.16 The mean and standard deviations of the estimated SFA, MUFA, and PUFA in the subcutaneous (o) and visceral (♦) adipose tissue of Iraqi-born and Swedish-born men.

Table 4.3 The mean and confidence intervals of estimated f_{SFA}, f_{MUFA}, and f_{PUFA} in visceral and subcutaneous adipose tissue of Iraqi- and Swedish-born men. The mean differences and confidence intervals between two groups (Iraqi-born – Swedish-born) and the corresponding *p*-values are also shown.

		Iraqi-born (n = 23)	Swedish-born (n = 14)	Difference	*p*-values
Subcutaneous adipose tissue	f_{SFA}	0.30 (CI 0.29–0.31)	0.35 (CI 0.33–0.36)	-0.05	< 0.001
	f_{MUFA}	0.53 (CI 0.51–0.55)	0.57 (CI 0.55–0.59)	-0.04	0.006
	f_{PUFA}	0.17 (CI 0.15–0.18)	0.09 (CI 0.07–0.10)	0.08	< 0.001
Visceral adipose tissue	f_{SFA}	0.30 (CI 0.29–0.31)	0.35 (CI 0.33–0.37)	-0.05	< 0.001
	f_{MUFA}	0.56 (CI 0.54–0.58)	0.58 (CI 0.56–0.61)	-0.02	0.1
	f_{PUFA}	0.14 (CI 0.13–0.15)	0.07 (CI 0.05–0.09)	0.07	< 0.001

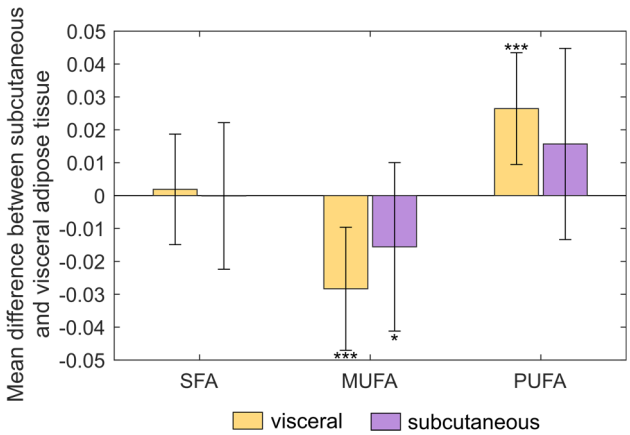

Figure 4.17 The mean difference of f_{SFA}, f_{MUFA}, and f_{PUFA} between subcutaneous and visceral adipose tissue (subcutaneous – visceral). */*** denotes significance value p < 0.05/0.001. A difference in f_{MUFA} was found among the Iraqi-born as well as the Swedish-born men. In contrast, no difference was found in f_{SFA} and a difference in f_{PUFA} was only found in the Iraqi-born men.

These result shows, for the first time, a difference in the FAC of subcutaneous and visceral adipose tissue between Iraqi- and Swedish-born men. The results of this study are consistent with the results from a previous study where lower levels of the fatty acids 12:0, 14:0, 16:0, and 18:1 (SFA and MUFA) and higher level fatty acid 18:2 (PUFA) were found in the plasma of Iraqi-born men compared to Swedish-born men (140). Although further studies are needed before the exact cause of the difference, or a possible association with dietary FAC or cardiovascular risk, may be concluded, the results presented here may help the understanding of the different cardiovascular risk profiles of the two groups.

Similar to other studies, differences in FAC between subcutaneous and visceral adipose tissue were found (38,68). Although the reason is not fully understood, it has been proposed that visceral and subcutaneous adipose tissue have different

metabolic functions (65). Furthermore, the estimated values of f_{SFA}, f_{MUFA}, and f_{MUFA} corresponds well with previous reported values using GC, MRI and MRS (0.24-0.38, 0.44-0.63, and 0.12-0.19, respectively (68,94,126)). Although the values may not be completely comparable due to differences in method used, investigated adipose tissue depot, and potential underlying disease, the results suggest that *in vivo* quantification of adipose tissue FAC using MRI is feasible. Thus, in this study, the unique possibility of high resolution, simultaneous multi-compartment, and non-invasive *in vivo* FAC quantification offered by the MRI method has been demonstrated.

5 Summary and outlook

In **Paper I**, a T_2-based fat quantification method using high resolution MR images was investigated. A 2-parameter fitting approach resulted in the best agreement and correlation to the reference method,low resolution water/fat imaging. Although long acquisition times may be a practical limitation, a T_2-based method offers the possibility of simultaneous estimation of *FF* and T_2-relaxation.

Using water/fat imaging, the intermuscular and intramuscular fat accumulation of lymphedema patients was assessed in **Paper II**. Excess fat volume was found in both compartments of the edematous limb. Further, the FAC of the subcutaneous adipose tissue of lymphedema patients were assessed using GC and MR-based methods (**Paper III**). Significantly different adipose tissue FAC was found between the edematous and healthy legs using both GC and MRI.

Methods for FAC quantification using MRS and MRI were compared to the gold standard, GC (**Paper III**). Generally strong correlations were found, especially for the MRI-based method. In addition, it was found that estimating FAC using a constrained *nmidb* had a negative impact on the estimated parameters in general, but the effect varied between MRS and MRI as well as between the various parameters.

In **Paper IV**, significantly lower f_{SFA} and higher f_{PUFA} were found in adipose tissue of Iraqi- compared to Swedish-born men in Sweden, using MRI. Additionally, a significant difference in FAC between visceral and subcutaneous adipose tissue was found, further demonstrating the feasibility of an MRI-based FAC quantification method where multiple adipose tissue depots can be assessed simultaneously.

5.1 Future work

Although this thesis reported a high correlation between the MRI-based method and GC, and showed that the MRI-based approach is a feasible method for *in vivo* estimation of adipose tissue FAC, there is still more work to be done in terms of optimizing and further improving the method. This includes the issue of the spatial variation seen in the frequency direction of the estimated FAC maps (see Figure 4.12 and Figure 4.15). Previous studies of FAC have reported a similar spatial variation using MRI (37,131) and MRS (125). While it has been suggested that the

artefact might be related to anti-aliasing filters (37) or asymmetric frequency response of the coil (131), definitive explanations and solutions are yet to be outlined and presented.

In the case of expressing *nmidb* and *cl* as functions of *ndb*, the results suggested a generally negative impact on the estimations, especially of f_{MUFA}, as discussed in section *4.6.3 Sources of bias*. Moreover, other expressions for *nmidb* and *cl* have been suggested (37,123), and further studies on which models should be used and if using constrained models affects the estimation of FAC in adipose tissue differently in various locations, are needed.

The excess fat accumulation found in the intermuscular and intramuscular compartments of lymphedema patients' limbs has not been shown previously. Thus, further investigations of the underlying mechanisms and potential effects of this are still needed. Similarly, the found difference between the FAC of adipose tissue in edematous and healthy legs of patients with lymphedema needs to be further investigated. While it has been suggested that the FAC is associated with chronic inflammation, the exact relationship was not explored further in this work.

Using MRI, a difference in FAC of subcutaneous and visceral adipose tissue between Iraqi-born and Swedish-born men has been demonstrated for the first time. This might be associated with the suggested difference in cardiovascular risk profiles between the groups (138). However, further studies are needed before any definite conclusions can be made.

5.2 Conclusions

In this thesis, the possibilities and limitations of MRI-based methods for fat content and FAC quantification have been explored with the following conclusions:

1. The T_2-based fat quantification approach showed good agreement with water/fat imaging, especially using a 2-parameter fit, and may thus be an alternative method for *FF* estimation using very high resolution MRI.
2. Excess fat was found in both the intramuscular and intermuscular compartment of edematous limb of lymphedema patients.
3. High correlations between the MR-based methods and the gold standard method, GC, were found. Especially the MRI-based method showed great potential for *in vivo* measurements of adipose tissue FAC.
4. Using the MRI-based method, significantly different FAC of Iraqi- and Swedish-born men was found in both visceral and subcutaneous adipose tissue. Also, significantly different FAC were found between the visceral and subcutaneous depots.

References

1. World Health Organization. Fact sheet on Obesity and Overweight. 2020;(April).
2. Al-Goblan AS, Al-Alfi MA, Khan MZ. Mechanism linking diabetes mellitus and obesity. Diabetes, Metab Syndr Obes Targets Ther. 2014;7:587–91.
3. Han TS, Al-Gindan YY, Govan L, Hankey CR, Lean MEJ. Associations of BMI, waist circumference, body fat, and skeletal muscle with type 2 diabetes in adults. Acta Diabetol. 2019;56(8):947–54.
4. Sarwar R, Pierce N, Koppe S. Obesity and nonalcoholic fatty liver disease: Current perspectives. Diabetes, Metab Syndr Obes Targets Ther. 2018;11(6):533–42.
5. Younossi Z, Anstee QM, Marietti M, Hardy T, Henry L, Eslam M, et al. Global burden of NAFLD and NASH: Trends, predictions, risk factors and prevention. Nat Rev Gastroenterol Hepatol. 2018;15(1):11–20.
6. Marengo A, Rosso C, Bugianesi E. Liver Cancer: Connections with Obesity, Fatty Liver, and Cirrhosis. Annu Rev Med. 2016;67(1):103–17.
7. Anandacoomarasamy A, Caterson I, Sambrook P, Fransen M, March L. The impact of obesity on the musculoskeletal system. Int J Obes. 2008;32(2):211–22.
8. Argolo DF, Hudis CA, Iyengar NM. The Impact of Obesity on Breast Cancer. Curr Oncol Rep. 2018;20(6).
9. Tchernof A, Després JP. Pathophysiology of human visceral obesity: An update. Physiol Rev. 2013;93(1):359–404.
10. Goodarzi MO. Genetics of obesity: what genetic association studies have taught us about the biology of obesity and its complications. Lancet Diabetes Endocrinol. 2018;6(3):223–36.
11. Kwok KHM, Lam KSL, Xu A. Heterogeneity of white adipose tissue: Molecular basis and clinical implications. Exp Mol Med. 2016;48(3).
12. Muller HL. Craniopharyngioma. Endocr Rev. 2014;35(3):513–43.
13. Gallagher D, Kuznia P, Heshka S, Albu J, Heymsfield SB, Goodpaster B, et al. Adipose tissue in muscle: A novel depot similar in size to visceral adipose tissue. Am J Clin Nutr. 2005;81(4):903–10.
14. Mattsson S, Thomas BJ. Development of methods for body composition studies. Phys Med Biol. 2006;51(13).
15. Fosbøl MO, Zerahn B. Contemporary methods of body composition measurement. Clin Physiol Funct Imaging. 2015;35(2):81–97.
16. Fang H, Berg E, Cheng X, Shen W, Hospital BT, Hospital BJ. How to best assess abdominal obesity. 2019;1–12.

17. Hu HH, Kan HE. Quantitative proton MR techniques for measuring fat. NMR Biomed. 2013;26(12):1609–29.
18. MacHann J, Horstmann A, Born M, Hesse S, Hirsch FW. Diagnostic imaging in obesity. Best Pract Res Clin Endocrinol Metab. 2013;27(2):261–77.
19. Mitra S, Fernandez-Del-Valle M, Hill JE. The role of MRI in understanding the underlying mechanisms in obesity associated diseases. Biochim Biophys Acta - Mol Basis Dis. 2017;1863(5):1115–31.
20. Reeder SB, Pineda AR, Wen Z, Shimakawa A, Yu H, Brittain JH, et al. Iterative decomposition of water and fat with echo asymmetry and least-squares estimation (IDEAL): Application with fast spin-echo imaging. Magn Reson Med. 2005;54(3):636–44.
21. Yu H, Shimakawa A, McKenzie CA, Brodsky E, Brittain JH, Reeder SB. Multiecho water-fat separation and simultaneous R*2 estimation with multifrequency fat spectrum modeling. Magn Reson Med. 2008;60(5):1122–34.
22. Reeder SB, McKenzie CA, Pineda AR, Yu H, Shimakawa A, Brau AC, et al. Water-fat separation with IDEAL gradient-echo imaging. J Magn Reson Imaging. 2007;25(3):644–52.
23. Dixon WT. Simple proton spectroscopic imaging. Radiology. 1984;153(1):189–94.
24. Kan HE, Scheenen TWJ, Wohlgemuth M, Klomp DWJ, van Loosbroek-Wagenmans I, Padberg GW, et al. Quantitative MR imaging of individual muscle involvement in facioscapulohumeral muscular dystrophy. Neuromuscul Disord. 2009;19(5):357–62.
25. Azzabou N, Sousa PL de, Caldas E, Carlier PG. Validation of a generic approach to muscle water T2 determination at 3T in fat-infiltrated skeletal muscle. J Magn Reson Imaging. 2015;41(3):645–53.
26. Marty B, Baudin PY, Reyngoudt H, Azzabou N, Araujo ECA, Carlier PG, et al. Simultaneous muscle water T2 and fat fraction mapping using transverse relaxometry with stimulated echo compensation. NMR Biomed. 2016;(29):431–43.
27. Hjelmgaard K, Eschen RB, Schmidt EB, Andreasen JJ, Lundbye-Christensen S. Fatty acid composition in various types of cardiac adipose tissues and its relation to the fatty acid content of atrial tissue. Nutrients. 2018;10(10).
28. Fritsche KL. The Science of Fatty Acids and Inflammation. Adv Nutr. 2015;6(3):293S-301S.
29. Puri P, Baillie RA, Wiest MM, Mirshahi F, Choudhury J, Cheung O, et al. A lipidomic analysis of nonalcoholic fatty liver disease. Hepatology. 2007;46(4):1081–90.
30. Leporq B, Lambert SA, Ronot M, Boucenna I, Colinart P, Cauchy F, et al. Quantification of triglyceride fatty acid composition in the fatty liver, subcutaneous and visceral adipose tissues with 3.0T MRI. Magn Reson Med. 2016;76(2):510–8.
31. Arendt BM, Comelli EM, Ma DWL, Lou W, Teterina A, Kim T, et al. Altered hepatic gene expression in nonalcoholic fatty liver disease is associated with lower hepatic n-3 and n-6 polyunsaturated fatty acids. Hepatology. 2015;61(5):1565–78.
32. Lewin AA, Storey P, Moccaldi M, Moy L, Gene Kim S. Fatty acid composition in

mammary adipose tissue measured by Gradient-echo Spectroscopic MRI and its association with breast cancers. Eur J Radiol. 2019;116(February):205–11.

33. Thakur SB, Horvat J V., Hancu I, Sutton OM, Bernard-Davila B, Weber M, et al. Quantitative in vivo proton MR spectroscopic assessment of lipid metabolism: Value for breast cancer diagnosis and prognosis. J Magn Reson Imaging. 2019;50(1):239–49.

34. Hamilton G, Yokoo T, Bydder M, Cruite I, Schroeder ME, Sirlin CB, et al. In vivo characterization of the liver fat 1H MR spectrum. NMR Biomed. 2011;24(7):784–90.

35. Berglund J, Ahlström H, Kullberg J. Model-Based Mapping of Fat Unsaturation and Chain Length by Chemical Shift Imaging — Phantom Validation and In Vivo Feasibility. 2012;1827:1815–27.

36. Peterson P, Månsson S. Simultaneous quantification of fat content and fatty acid composition using MR imaging. Magn Reson Med. 2013;69(3):688–97.

37. Bydder M, Girard O, Hamilton G. Mapping the double bonds in triglycerides. Magn Reson Imaging. 2011;29(8):1041–6.

38. Machann J, Stefan N, Wagner R, Bongers M, Schleicher E, Fritsche A, et al. Intra- and interindividual variability of fatty acid unsaturation in six different human adipose tissue compartments assessed by 1H-MRS in vivo at 3 T. NMR Biomed. 2017;30(9):1–10.

39. Martel D, Leporq B, Bruno M, Regatte RR, Honig S, Chang G. Chemical shift-encoded MRI for assessment of bone marrow adipose tissue fat composition: Pilot study in premenopausal versus postmenopausal women. Magn Reson Imaging. 2018;53(January):148–55.

40. Lundbom J, Hakkarainen A, Lundbom N, Taskinen MR. Deep subcutaneous adipose tissue is more saturated than superficial subcutaneous adipose tissue. Int J Obes. 2013;37(4):620–2.

41. Marlatt KL, Ravussin E. METABOLISM (CJ BILLINGTON, SECTION EDITOR) Brown Adipose Tissue: an Update on Recent Findings. 2017;389–96.

42. Sharma AM. Adipose tissue: A mediator of cardiovascular risk. Int J Obes. 2002;26:S5–7.

43. Wronska A, Kmiec Z. Structural and biochemical characteristics of various white adipose tissue depots. Acta Physiol. 2012;205(2):194–208.

44. Lapidus L, Bengtsson C, Larsson B, Pennert K, Rybo E, Sjöström L. Distribution of adipose tissue and risk of cardiovascular disease and death: A 12 year follow up of participants in the population study of women in Gothenburg, Sweden. Br Med J. 1984;289(6454):1257–61.

45. Bjorntorp P. "Portal" adipose tissue as a generator of risk factors for cardiovascular disease and diabetes. Arteriosclerosis. 1990;10(4):493–6.

46. Levelt E, Pavlides M, Banerjee R, Mahmod M, Kelly C, Sellwood J, et al. Ectopic and Visceral Fat Deposition in Lean and Obese Patients with Type 2 Diabetes. J Am Coll Cardiol. 2016;68(1):53–63.

47. Ross R, Freeman J, Hudson R, Janssen I. Abdominal obesity, muscle composition,

and insulin resistance in premenopausal women. J Clin Endocrinol Metab. 2002;87(11):5044–51.

48. Snijder MB, van Dam RM, Visser M, Seidell JC. What aspects of body fat are particularly hazardous and how do we measure them? Int J Epidemiol. 2006;35(1):83–92.

49. Zamboni M, Rossi AP, Fantin F, Budui SL, Zoico E, Zamboni GA, et al. Predictors of Ectopic Fat in Humans. Curr Obes Rep. 2014;3(4):404–13.

50. Kohli S, Lear S a. Differences in subcutaneous abdominal adiposity regions in four ethnic groups. Obesity (Silver Spring). 2013;21(11):2288–95.

51. Hamrick MW, McGee-Lawrence ME, Frechette DM. Fatty Infiltration of Skeletal Muscle: Mechanisms and Comparisons with Bone Marrow Adiposity. Front Endocrinol (Lausanne). 2016;7(June):69.

52. Wajchenberg BL, Lé B, Wajchenberg O. Subcutaneous and Visceral Adipose Tissue : Endocr Rev. 2000;21(6):697–738.

53. Reeder SB, Cruite I, Hamilton G, Sirlin CB. Quantitative assessment of liver fat with magnetic resonance imaging and spectroscopy. J Magn Reson Imaging. 2011;34(4):729–49.

54. Hu HH, Kim H-W, Nayak KS, Goran MI. Comparison of fat–water MRI and single-voxel MRS in the assessment of hepatic and pancreatic fat fractions in humans. Obesity. 2010;18(4):841–7.

55. Goodpaster BH, Kelley DE. Skeletal muscle triglyceride: marker or mediator of obesity-induced insulin resistance in type 2 diabetes mellitus? Curr Diab Rep. 2002;2(3):216–22.

56. Carlier PG, Marty B, Scheidegger O, Loureiro de Sousa P, Baudin P-Y, Snezhko E, et al. Skeletal Muscle Quantitative Nuclear Magnetic Resonance Imaging and Spectroscopy as an Outcome Measure for Clinical Trials. J Neuromuscul Dis. 2016;3(1):1–28.

57. Reeder SB, Sirlin CB. Quantification of liver fat with magnetic resonance imaging. Vol. 18, Magnetic Resonance Imaging Clinics of North America. 2010. p. 337–57.

58. Bhatt HB, Smith RJ. Fatty liver disease in diabetes mellitus. Hepatobiliary Surg Nutr. 2015;4(2):101–8.

59. Goodpaster BH, Wolf D. Skeletal muscle lipid accumulation in obesity, insulin resistance, and type 2 diabetes. Pediatr Diabetes. 2004;5(4):219–26.

60. Shulman GI. Ectopic fat in insulin resistance, dyslipidemia, and cardiometabolic disease. N Engl J Med. 2014;371(12):1131–41.

61. Birkenfeld AL, Shulman GI. Nonalcoholic fatty liver disease, hepatic insulin resistance, and type 2 Diabetes. Hepatology. 2014;59(2):713–23.

62. Marinou K, Hodson L, Vasan SK, Fielding BA, Banerjee R, Brismar K, et al. Structural and Functional Properties of Deep Abdominal Subcutaneous Adipose Tissue Explain Its Association With Insulin Resistance and Cardiovascular Risk in Men. Diabetes Care. 2014;37(3):821–9.

63. Bastien M, Poirier P, Lemieux I, Després JP. Overview of epidemiology and contribution of obesity to cardiovascular disease. Prog Cardiovasc Dis.

2014;56(4):369–81.

64. Damon BM, Li K, Bryant ND. Magnetic resonance imaging of skeletal muscle. Handb Clin Neurol. 2016;136:827–42.

65. Ibrahim MM. Subcutaneous and visceral adipose tissue: Structural and functional differences. Obes Rev. 2010;11(1):11–8.

66. Cancello R, Zulian A, Gentilini D, Maestrini S, Della Barba A, Invitti C, et al. Molecular and morphologic characterization of superficial-and deep-subcutaneous adipose tissue subdivisions in human obesity. Obesity. 2013;21(12):2562–70.

67. Tordjman J, Divoux A, Prifti E, Poitou C, Pelloux V, Hugol D, et al. Structural and inflammatory heterogeneity in subcutaneous adipose tissue: Relation with liver histopathology in morbid obesity. J Hepatol. 2012;56(5):1152–8.

68. Hodson L, Skeaff CM, Fielding BA. Fatty acid composition of adipose tissue and blood in humans and its use as a biomarker of dietary intake. Prog Lipid Res. 2008;47(5):348–80.

69. Addison O, Marcus RL, Lastayo PC, Ryan AS. Intermuscular fat: A review of the consequences and causes. Int J Endocrinol. 2014;2014:34–6.

70. Stinkens R, Goossens GH, Jocken JWE, Blaak EE. Targeting fatty acid metabolism to improve glucose metabolism. Obes Rev. 2015;16(9):715–57.

71. Simon NG, Noto YI, Zaidman CM. Skeletal muscle imaging in neuromuscular disease. J Clin Neurosci. 2016;33:1–10.

72. Deenen JCW, Horlings CGC, Verschuuren JJGM, Verbeek ALM, Van Engelen BGM. The epidemiology of neuromuscular disorders: A comprehensive overview of the literature. J Neuromuscul Dis. 2015;2(1):73–85.

73. Tuttle LJ, Sinacore DR, Mueller MJ. Intermuscular adipose tissue is muscle specific and associated with poor functional performance. J Aging Res. 2012;2012.

74. Boesch C, Machann J, Vermathen P, Schick F. Role of proton MR for the study of muscle lipid metabolism. NMR Biomed. 2006 Nov;19(7):968–88.

75. Goodpaster BH, He J, Watkins S, Kelley DE. Skeletal muscle lipid content and insulin resistance: Evidence for a paradox in endurance-trained athletes. J Clin Endocrinol Metab. 2001;86(12):5755–61.

76. Zhiqiang L. NIH Public Access. Magn Reson Med. 2009;61(6):1415–24.

77. Leporq B, Lambert SA, Ronot M, Vilgrain V, Van Beers BE. Simultaneous MR quantification of hepatic fat content, fatty acid composition, transverse relaxation time and magnetic susceptibility for the diagnosis of non-alcoholic steatohepatitis. NMR Biomed. 2017;30(10):1–8.

78. Erickson ML, Haus JM, Malin SK, Flask CA, McCullough AJ, Kirwan JP. Non-invasive assessment of hepatic lipid subspecies matched with non-alcoholic fatty liver disease phenotype. Nutr Metab Cardiovasc Dis. 2019;29(11):1197–204.

79. Johnson NA, Walton DW, Sachinwalla T, Thompson CH, Smith K, Ruell PA, et al. Noninvasive assessment of hepatic lipid composition: Advancing understanding and management of fatty liver disorders. Hepatology. 2008;47(5):1513–23.

80. Patsch JM, Li X, Baum T, Yap SP, Karampinos DC, V SA, et al. Bone Marrow Fat Composition as a Novel Imaging Biomarker in Postmenopausal Women With

Prevalent Fragility Fractures. J Bone Miner Res. 2013;28(8):1721–8.

81. Yeung DKW, Griffith JF, Antonio GE, Lee FKH, Woo J, Leung PC. Osteoporosis is associated with increased marrow fat content and decreased marrow fat unsaturation: A proton MR spectroscopy study. J Magn Reson Imaging. 2005;22(2):279–85.

82. Baum T, Yap SP, Karampinos DC, Nardo L, Kuo D, Burghardt AJ, et al. Does vertebral bone marrow fat content correlate with abdominal adipose tissue, lumbar spine bone mineral density, and blood biomarkers in women with type 2 diabetes mellitus? J Magn Reson Imaging. 2012;35(1):117–24.

83. Freed M, Storey P, Lewin AA, Babb J, Moccaldi M, Moy L, et al. Evaluation of breast lipid composition in patients with benign tissue and cancer by using multiple gradient-echo MR imaging. Radiology. 2016;281(1):43–53.

84. Ailhaud G, Guesnet P. Fatty acid composition of fats is an early determinant of childhood obesity: A short review and an opinion. Obes Rev. 2004;5(1):21–6.

85. Acosta-Montaño P, García-González V. Effects of dietary fatty acids in pancreatic beta cell metabolism, implications in homeostasis. Nutrients. 2018;10(4):1–14.

86. Lecerf JM. Fatty acids and cardiovascular disease. Nutr Rev. 2009;67(5):273–83.

87. Briggs M, Petersen K, Kris-Etherton P. Saturated Fatty Acids and Cardiovascular Disease: Replacements for Saturated Fat to Reduce Cardiovascular Risk. Healthcare. 2017;5(2):29.

88. Hedrick VE, Dietrich AM, Estabrooks PA, Savla J, Serrano E, Davy BM. Dietary biomarkers: advances, limitations and future directions. Nutr J. 2012;11.

89. Karampinos DC, Baum T, Nardo L, Alizai H, Yu H, Carballido-Gamio J, et al. Characterization of the regional distribution of skeletal muscle adipose tissue in type 2 diabetes using chemical shift-based water/fat separation. J Magn …. 2012;35(4):899–907.

90. Nardo L, Karampinos DC, Lansdown DA, Carballido-Gamio J, Lee S, Maroldi R, et al. Quantitative assessment of fat infiltration in the rotator cuff muscles using water-fat MRI. J Magn Reson Imaging. 2014;39(5):1178–85.

91. Hoffner M, Peterson P, Månsson S, Brorson H. Lymphedema Leads to Fat Deposition in Muscle and Decreased Muscle/Water Volume After Liposuction: A Magnetic Resonance Imaging Study. Lymphat Res Biol. 2018;16(2):174–81.

92. Dodds ED, McCoy MR, Rea LD, Kennish JM. Gas chromatographic quantification of fatty acid methyl esters: Flame ionization detection vs. electron impact mass spectrometry. Lipids. 2005;40(4):419–28.

93. Ren J, Dimitrov I, Sherry a D, Malloy CR. Composition of adipose tissue and marrow fat in humans by 1H NMR at 7 Tesla. J Lipid Res. 2008;49(9):2055–62.

94. Lundbom J, Hakkarainen A, Fielding B, Söderlund S, Westerbacka J, Taskinen MR, et al. Characterizing human adipose tissue lipids by long echo time 1H-MRS in vivo at 1.5 Tesla: Validation by gas chromatography. NMR Biomed. 2010;23(5):466–72.

95. Strobel K, Van Den Hoff J, Pietzsch J. Localized proton magnetic resonance spectroscopy of lipids in adipose tissue at high spatial resolution in mice in vivo. J Lipid Res. 2008;49(2):473–80.

96. Leporq B, Lambert SA, Ronot M, Vilgrain V, Van Beers BE. Quantification of the triglyceride fatty acid composition with 3.0 T MRI. NMR Biomed. 2014;27(10):1211–21.

97. Yu H, McKenzie CA, Shimakawa A, Vu AT, Brau ACS, Beatty PJ, et al. Multiecho reconstruction for simultaneous water-fat decomposition and T2* estimation. J Magn Reson Imaging. 2007;26(4):1153–61.

98. Yu H, Shimakawa A, Hines CDG, McKenzie CA, Hamilton G, Sirlin CB, et al. Combination of complex-based and magnitude-based multiecho water-fat separation for accurate quantification of fat-fraction. Magn Reson Med. 2011;66(1):199–206.

99. Ma J. Dixon techniques for water and fat imaging. J Magn Reson Imaging. 2008;28(3):543–58.

100. Berglund J, Ahlström H, Johansson L, Kullberg J. Two-point dixon method with flexible echo times. Magn Reson Med. 2011;65(4):994–1004.

101. Eggers H, Börnert P. Chemical shift encoding-based water-fat separation methods. J Magn Reson Imaging. 2014;40(2):251–68.

102. Peterson P. Fat quantification using multiecho sequences with bipolar gradients: Investigation of accuracy and noise performance. Magn Reson Med. 2014;71(1):219–29.

103. Bydder M, Yokoo T, Hamilton G, Middleton MS, Chavez AD, Schwimmer JB, et al. Relaxation effects in the quantification of fat using gradient echo imaging. Magn Reson Imaging. 2008;26(3):347–59.

104. Månsson S, Peterson P, Johansson E. Quantification of low fat contents: A comparison of MR imaging and spectroscopy methods at 1.5 and 3 T. Magn Reson Imaging. 2012;30(10):1461–7.

105. Torriani M, Townsend E, Thomas BJ, Bredella MA, Ghomi RH, Tseng BS. Lower leg muscle involvement in Duchenne muscular dystrophy: An MR imaging and spectroscopy study. Skeletal Radiol. 2012;41(4):437–45.

106. Tasca G, Monforte M, Ottaviani P, Pelliccioni M, Frusciante R, Laschena F, et al. Magnetic resonance imaging in a large cohort of facioscapulohumeral muscular dystrophy patients: Pattern refinement and implications for clinical trials. Ann Neurol. 2016;79(5):854–64.

107. Friedman SD, Poliachik SL, Carter GT. Muscle-fat magnetic resonance imaging: Applications. Muscle and Nerve. 2014;50(2):157–8.

108. Azzabou N, De Sousa PL, Caldas E, Carlier PG. Validation of a generic approach to muscle water T2 determination at 3T in fat-infiltrated skeletal muscle. J Magn Reson Imaging. 2015;41(3):645–53.

109. Kamman RL, Bakker CJG, Van Dijk P, Stomp GP, Heiner AP, Berendsen HJC. Multi-exponential relaxation analysis with MR imaging and NMR spectroscopy using fat-water systems. Magn Reson Imaging. 1987;5(1):381–92.

110. Bromage GE. A quantification of the hazards of fitting sums of exponentials to noisy data. Comput Phys Commun. 1983;30(3):229–33.

111. Barbieri S, Donati OF, Froehlich JM, Thoeny HC. Impact of the calculation

algorithm on biexponential fitting of diffusion-weighted MRI in upper abdominal organs. Magn Reson Med. 2016;75(5):2175–84.

112. Neal RM. Slice sampling. Ann Stat. 2003;31(3):758–67.

113. Gold GE, Han E, Stainsby J, Wright G, Brittain J, Beaulieu C. Musculoskeletal MRI at 3.0 T: Am J Roentgenol. 2004;(183):343–51.

114. Klupp E, Weidlich D, Schlaeger S, Baum T, Cervantes B, Deschauer M, et al. B1-insensitive T2 mapping of healthy thigh muscles using a T2-prepared 3D TSE sequence. PLoS One. 2017;12(2):e0171337.

115. Dayan JH, Ly CL, Kataru RP, Mehrara BJ. Lymphedema : Pathogenesis and Novel Therapies. 2018;(August 2017):1–14.

116. Brorson H, Svensson H. Complete reduction of lymphoedema of the arm by liposuction after breast cancer. Scand J Plast Reconstr Surg hand Surg. 1997;31(2):137–43.

117. Brorson H. LIPOSUCTION IN ARM LYMPHEDEMA TREATMENT. Scand J Surg. 2003;(92):287–95.

118. Cucchi F, Rossmeislova L, Simonsen L, Jensen MR, Bülow J. A vicious circle in chronic lymphoedema pathophysiology? An adipocentric view. Obes Rev. 2017;18(10):1159–69.

119. Hoffner M, Bagheri S, Hansson E, Manjer J, Troëng T, Brorson H. SF-36 Shows Increased Quality of Life Following Complete Reduction of Postmastectomy Lymphedema with Liposuction. Lymphat Res Biol. 2017;15(1):87–98.

120. Brorson H. Liposuction in Lymphedema Treatment. J Reconstr Microsurg. 2015;32(1):56–65.

121. Brorson H, Svensson H. Liposuction combined with controlled compression therapy reduces arm lymphedema more effectively than controlled compression therapy alone. Plast Reconstr Surg. 1998;102(4):1058-67;

122. Amore M, Tapia L, Mercado D, Pattarone G, Ciucci J. Lymphedema: A General Outline of Its Anatomical Base. J Reconstr Microsurg. 2015;32(1):2–9.

123. Berglund J, Rydén H, Skorpil M. Increased measurement precision for fatty acid composition mapping by parameter reduction. In Proceedings of the 24th Annual Meeting of ISMRM, Singapore, Singapore, 2016. Abstract 3271.

124. Hamilton G, Smith DL, Bydder M, Nayak KS, Hu HH. MR properties of brown and white adipose tissues. J Magn Reson Imaging. 2011;34(2):468–73.

125. Hamilton G, Schlein AN, Middleton MS, Hooker CA, Wolfson T, Gamst AC, et al. In Vivo Triglyceride Composition of Abdominal Adipose Tissue Measured by H MRS at 3T. 2017;45(5):1455–63.

126. Nemeth A, Segrestin B, Leporq B, Seyssel K, Faraz K, Sauvinet V, et al. 3D Chemical Shift-Encoded MRI for Volume and Composition Quantification of Abdominal Adipose Tissue During an Overfeeding Protocol in Healthy Volunteers. J Magn Reson Imaging. 2019;49(6):1587–99.

127. Hamilton G, Middleton MS, Bydder M, Yokoo T, Schwimmer JB, Kono Y, et al. Effect of PRESS and STEAM sequences on magnetic resonance spectroscopic liver fat quantification. J Magn Reson Imaging. 2009;30(1):145–52.

128. Ruschke S, Kienberger H, Baum T, Kooijman H, Settles M, Haase A, et al. Diffusion-weighted stimulated echo acquisition mode (DW-STEAM) MR spectroscopy to measure fat unsaturation in regions with low proton-density fat fraction. Magn Reson Med. 2016;75(1):32–41.

129. Fairgrieve-Park L, Fallone CJ, Yahya A. Long TE PRESS and STEAM for measuring the triglyceride glycerol CH2 protons at 3 T. NMR Biomed. 2019;32(1):1–8.

130. Froeling M, Hughes E, Schlaffke L, Kan HE, Hollingsworth KG. The relation between fat calibration in multi-echo spin-echo water T2 mapping and STEAM fat T2 relaxation measurements. In Proceedings of the 27th Annual Meeting of ISMRM, Montréal, Canada, 2019. Abstract 1273.

131. Schneider M, Janas G, Lugauer F, Hoppe E, Nickel D, Dale BM, et al. Accurate fatty acid composition estimation of adipose tissue in the abdomen based on bipolar multi-echo MRI. Magn Reson Med. 2019;81(4):2330–46.

132. Peterson P, Svensson J, Månsson S. Relaxation effects in MRI-based quantification of fat content and fatty acid composition. Magn Reson Med. 2014;72(5):1320–9.

133. Ly CL, Kataru RP, Mehrara BJ. Inflammatory manifestations of lymphedema. Int J Mol Sci. 2017;18(1):1–13.

134. Liu L, Mei M, Yang S, Li Q. Roles of chronic low-grade inflammation in the development of ectopic fat deposition. Mediators Inflamm. 2014;2014.

135. Innes JK, Calder PC. Prostaglandins , Leukotrienes and Essential Fatty Acids Omega-6 fatty acids and in fl ammation. 2019;132(March 2018):41–8.

136. Mattacks CA, Sadler D, Pond CM. The cellular structure and lipid/protein composition of adipose tissue surrounding chronically stimulated lymph nodes in rats. J Anat. 2003;202(6):551–61.

137. Pond CM, Mattacks CA. The source of fatty acids incorporated into proliferating lymphoid cells in immune-stimulated lymph nodes. Br J Nutr. 2003;89(3):375–82.

138. Bennet L, Nilsson PM. Country of birth modifies the associations of body mass and hemoglobin A1c with office blood pressure in Middle Eastern immigrants and native Swedes. J Hypertens. 2014;32(12):2362–70.

139. Yusuf S, Hawken S, Ounouu S, Dans T, Avezum A, Lanas F, et al. Effect of potentially modifiable risk factors associated with myocardial infarction in 52 countries (the INTERHEART study): case-control study. Lancet. 2004;364:937–52.

140. Al-Majdoub M, Spégel P, Bennet L. Metabolite profiling paradoxically reveals favorable levels of lipids, markers of oxidative stress and unsaturated fatty acids in a diabetes susceptible group of Middle Eastern immigrants. Acta Diabetol. 2019;(0123456789).

141. Fattore E, Massa E. Dietary fats and cardiovascular health: a summary of the scientific evidence and current debate. Int J Food Sci Nutr. 2018;69(8):916–27.

142. Bazzano LA, Green T, Harrison TN, Reynolds K. Dietary approaches to prevent hypertension. Curr Hypertens Rep. 2013;15(6):694–702.

143. Rasmussen BM, Vessby B, Uusitupa M, Berglund L, Pedersen E, Riccardi G, et al. Effects of dietary saturated, monounsaturated, and n-3 fatty acids on blood pressure

in healthy subjects. Am J Clin Nutr. 2006;83(2):221–6.

144. Schwingshackl L, Strasser B, Hoffmann G. Effects of monounsaturated fatty acids on cardiovascular risk factors: A systematic review and meta-analysis. Ann Nutr Metab. 2011;59(2–4):176–86.

145. Gillingham LG, Harris-Janz S, Jones PJH. Dietary monounsaturated fatty acids are protective against metabolic syndrome and cardiovascular disease risk factors. Lipids. 2011;46(3):209–28.

146. Erkkilä A, de Mello VDF, Risérus U, Laaksonen DE. Dietary fatty acids and cardiovascular disease: An epidemiological approach. Prog Lipid Res. 2008;47(3):172–87.

147. Naska A, Lagiou A, Lagiou P. Dietary assessment methods in epidemiological research: Current state of the art and future prospects. F1000Research. 2017;6(0):1–8.

148. Shim J-S, Oh K, Kim HC. Dietary assessment methods in epidemiologic studies. Epidemiol Health. 2014;36(2):1–8.

Printed by Media-Tryck, Lund 2020 NORDIC SWAN ECOLABEL 3041 0903

LUND UNIVERSITY

FACULTY OF MEDICINE

Department of Translational Medicine

Lund University, Faculty of Medicine
Doctoral Dissertation Series 2020:68
ISBN 978-91-7619-929-9
ISSN 1652-8220